Functional and molecular characterisation of a unique double homozygous variant causing ABCA4-related retinopathy

Mari Hamre Bu

This thesis is submitted in partial fulfilment of the requirements for the degree of Master of Science

Department of Biological Sciences
Faculty of Mathematics and Natural Sciences
University of Bergen

Department of Medical Genetics
Haukeland University Hospital

June 2023

Acknowledgments

I would like to express my sincere gratitude for the support and guidance I received this last year at the Department of Medical Genetics at Haukeland University Hospital.

First and foremost, I am deeply thankful to my main supervisors, Per Morten Knappskog and Eirik Bratland. Your expertise, guidance, and constructive feedback significantly shaped this project, and I am very grateful for your support and positivity throughout this entire process. I would also like to extend my gratitude to my co-supervisor, Sigrid Aslaksen, for your invaluable input and guidance when it comes to both writing and techniques in the lab.

My heartfelt thanks go to Hilde Eldevik Rusaas for your extensive guidance in the laboratory. Your continuous patience and positivity were instrumental in providing me with the tools I needed to succeed in the lab. Additionally, I would like to express my gratitude to Marie Hagen for teaching me various lab techniques with kindness and encouragement.

I am very grateful to my family and friends for your continuous support and motivation. Your belief in me and constant encouragement to do my best, inspired me throughout the work with this thesis. Lastly, I would like to thank my fellow master's students for your wonderful company and support in the study hall. Your company thankfully made the writing process more enjoyable.

Thank you all for being an integral part of this project and for your positivity, contributions, encouragement, and support!

Bergen, June 2023
Mari Hamre Bu

Table of contents

List of Abbreviations

ABCA4	ATP binding cassette protein, subfamily A member 4
AR	Autosomal recessive
BSA	Bovine serum albumin
Cryo-EM	Cryogenic electron microscopy
DAPI	Diamond Antifade Mountant with 4′,6-diamidino-2-phenylindole
DMEM	Dulbecco's Modified Eagle
dNTP	Deoxynucleoside triphasphate
ECD	Exocytoplasmic domain
EH	Extracellular α-helices
ER	Endoplasmic reticulum
EV	Empty vector
FBS	Fetal Bovine Serum
HF	High fidelity
HRP	Horseradish Peroxidase
IRD	Inherited retinal dystrophy
LB	Luria Bertani
LF PVDF	Low fluorescence polyvinylidene difluoride
m-IgGK BP	mouse IgG kappa binding protein
MEM NEAA	Minimum Essential Medium Non-Essential Amino Acids
N-Ret-PE	N-retinyledene-phosphatidylethenolamine
NADPH	Nicotinamide adenine dinucleotide phosphate
NBD	Nucleotide binding domain
OCT	Optical coherence tomography
ON	Overnight
PB	Phosphate Buffer
PBS	Phosphate buffered saline
PCR	Polymerase chain reaction
PE	Phosphatidylethanolamine
PFA	Paraformaldehyde
PH	Pinning helices
qPCR	Real-time PCR
RD	Regulatory domain
RDH	Retinol dehydrogenase
RDH8	Retinol dehydrogenase 8
RPE	Retinal pigment epithelial
rpm	Revolutions per minute
RT	Room temperature
S.O.C.	Super Optimal Broth
SDS-PAGE	Sodium dodecyl sulphate-polyacrylamide gel electrophoresis
TMD	Transmembrane domain
VFVNFA	Val-Phe-Val-Asn-Phe-Ala
WT	Wild-type

Abstract

Inherited retinal dystrophies (IRDs) constitute a diverse group of genetic diseases that are characterised by degeneration of the retina, causing progressive vision loss. IRDs are caused by deficiencies in the visual cycle where photons are translated into nerve signals. An important process in the visual cycle is the removal of excess N-Ret-PE, performed by the transmembrane ABCA4 protein which is located in disc-like structures in the outer regions of photoreceptors. Mutations in the *ABCA4* gene are the cause of functionally altered ABCA4-proteins, which in turn lead to the loss of photoreceptors in the retina. There is a large scope of pathogenic variants of *ABCA4,* and the disease manifests with a variety of phenotypes.

A patient under clinical investigation at Haukeland University Hospital was diagnosed with a severe phenotype of ABCA4-retinopathy, caused by homozygosity for a doubly mutated allele. In this study, the aim was to characterise the two variants located on the same allele, c.5882G>A, p.(Gly1961Glu) and c.634C>T p.(Arg212Cys) as single variants as well as the double mutation. The functional characterisation was carried out using several methods which included investigating the mRNA and protein expression, as well as the intracellular localisation of the ABCA4 variants. The functional characterisation of the double variant, including protein expression, mRNA expression and subcellular localisation exhibited results that were similar to WT ABCA4. Additionally, the impact on the protein 3D-structure of the mutations on the ABCA4 protein was investigated through molecular modelling. This indicated a potential of the two investigated mutations to disrupt amino acid interactions and impact protein stability, and that they likely contribute to decreased ATPase activity, possibly through a synergistic effect of the mutations occurring in different domains of the protein.

The results from the partial functional characterisation do not explain the severe phenotype observed in the patient. This discrepancy indicated that the methods used to characterise the variant here were insufficient in explaining the cause of the phenotype. Therefore, to further investigate the double variant, a new ATPase activity assay to study the double variant should be developed, and the mRNA expression in the patient's fibroblasts should be studied.

1. Introduction

1.1 Vision

1.1.1 The eye

The human eye is a complex organ that is responsible for vision. It consists of several structures that all have a specific function. As presented in Figure 1.1A, the basic structure of the eye includes components such as the cornea, the pupil, the lens, the retina, the macula and fovea, and the optic nerve. Light passes through the pupil and crosses the lens, which is crucial in providing added focus. The light passes through the vitreous humour and enters the retina from the inside of the eye. The retina consists of several layers, including a layer of photoreceptor cells, cones and rods, as well as a layer of ganglion cells, in addition to other layers with bipolar cells, amacrine cells and horizontal cells. When the light enters the retina, it passes through the ganglion cell layer before reaching the photoreceptors. In the macula, the minute area called the fovea is especially capable of acute and detailed vision. The rods and cones, that are spread within their layer throughout the retina, are narrow cells consisting of the outer segment, the inner segment, the nucleus, and the synaptic body as presented in Figure 1.1B. The outer segments of the photoreceptors are filled with a large number of discs, that are infolded shelves of cell membrane (Hall, 2011).

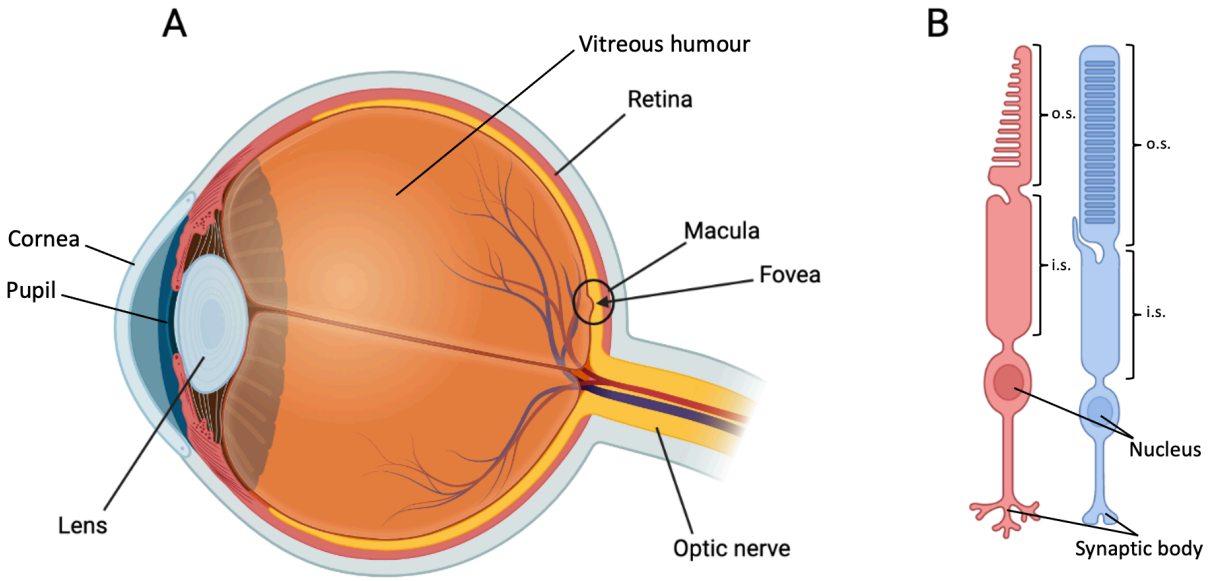

Figure 1.1: Figure depicting different components of the eye. A: Simplified sagittal diagram of the human eye, with markings localising the cornea, the lens, the pupil, the vitreous humour, the retina, the fovea within the macula and the optic nerve. **B:** Simplified diagram of photoreceptors cone (red) and rod (blue) cells, with disc-like structures in their outer regions, both consisting of outer segments, inner segments, nucleus, and a synaptic body that all work together in the conversion of a photon into a nerve signal. o.s.: outer segments, i.s.: inner segments. The figure was created using BioRender.com

1.1.2 The visual cycle

The process where a photon enters the eye and is converted into a nerve signal is called phototransduction. The photon passes through the eye and enters the discs of the cone and rod photoreceptors. Within the discs, rhodopsin and cone opsin are photosensitive pigments that will induce phototransduction when photons enter the photoreceptors (Saari, 2000; Wang & Kefalov, 2011). Rhodopsin consists of 11-*cis*-retinal covalently bound to opsin. As seen in Figure 1.2, when a photon is absorbed in the rod cells, 11-*cis*-retinal is isomerized to all-*trans*-retinal and released from opsin. Free all-*trans*-retinal is largely released to the cytoplasmic leaflet of the membrane. Retinol dehydrogenase 8 (RDH8) reduces all-*trans*-retinal to all-*trans*-retinol by reduced nicotinamide adenine dinucleotide phosphate (NADPH). Then, all-*trans*-retinol is transported out of the disc to retinal pigment epithelial cells (RPE), to be converted back into 11-*cis*-retinal through a series of reactions. 11-*cis*-retinal is transported back into the disc membrane, covalently binds to opsin to form rhodopsin, and allows for a new visual cycle (Sun et al., 1999; Saari, 2012; Weng et al., 1999).

The visual cycle also occurs in cone photoreceptors. In the cone cells, the disc-like structures are not closed membranes as in the rod cells, but rather contiguous infoldings of the plasma membrane in the outer parts of the cells (Ding et al., 2015). Here, cone opsin is light activated and all-*trans*-retinal is released and reduced to all-*trans*-retinol by RDH8 as in the rod cells. For these cells, all-*trans*-retinol is either transported to RPE where it follows the visual cycle as explained for rod cells, or to Müeller cells. In the Müeller cells, all-*trans*-retinol is enzymatically converted to 11-*cis*-retinol, which is transferred back to the inner segment of the cone cells. 11-*cis*-retinol then moves to the outer segments where it is oxidised by an unidentified retinol dehydrogenase (RDH) to 11-*cis*-retinal for pigment regeneration (Wang & Kefalov, 2011).

For both visual cycles, some of all-*trans*-retinal is not directly reduced to all-*trans*-retinol by RDH8 and is therefore kept within the disc membrane (Molday et al., 2022). This induces a reaction between the excess all-*trans*-retinal and phosphatidylethanolamine (PE), producing N-retinyledene-PE (N-Ret-PE) within the photoreceptor disc membrane (Anderson & Maude, 1970; Poincelot et al., 1969). In a normal functioning visual cycle, N-Ret-PE is removed from the lumen of the disc membranes of rods to the cytoplasmic leaflet of the disc membrane (Figure 1.2). For cone cells, N-Ret-PE is transported from the extracellular side of the membrane to the cytoplasmic leaflet. This crucial transportation process is performed by the transmembrane disc

protein ABCA4, which is an ATP-binding cassette protein, in subfamily A as member 4 (Beharry et al., 2004).

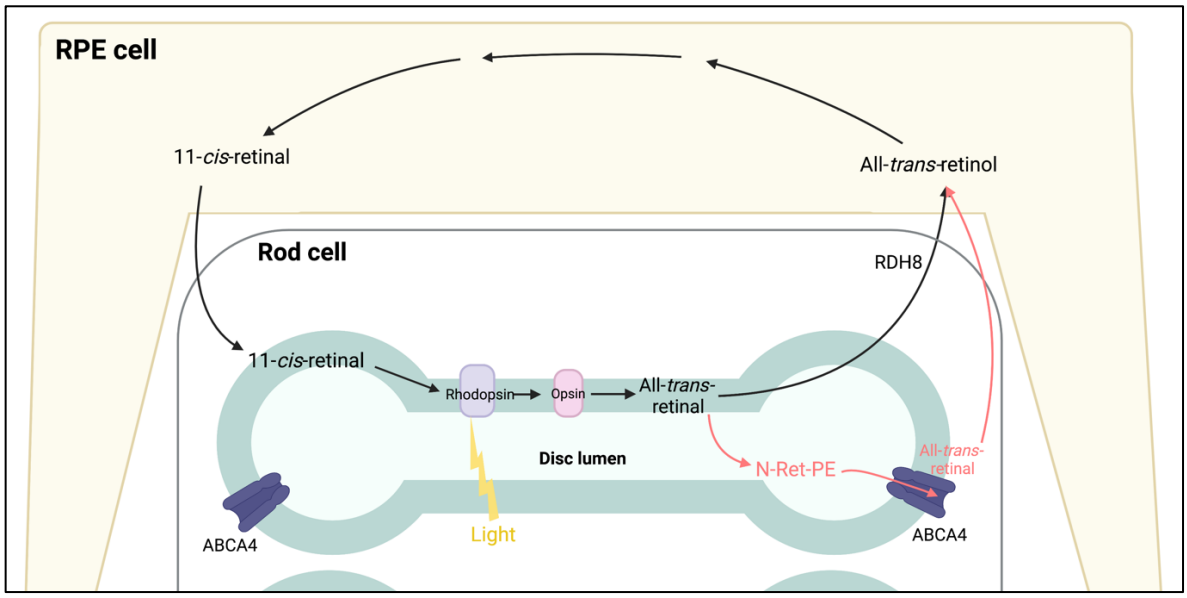

Figure 1.2: **Simplified overview of selected important reactions in the rod visual cycle.** Depicted in the figure are parts of the outer segment of a rod photoreceptor cell containing disc-like structures. The photoreceptor cell is in close contact with an RPE cell. The visual cycle happens here. A photon enters the photoreceptor, which leads to the isomerization of 11-*cis*-retinal in rhodopsin into all-*trans*-retinal, and release of opsin. Most of the all-*trans*-retinal is reduced to all-*trans*-retinol by RDH8, and transported to the RPE cell. Through a series of reactions, all-*trans*-retinol is reduced back to 11-*cis*-retinal which is transported back into the disc-like structure within the rod cell where it binds to opsin and forms rhodopsin. Some of all-*trans*-retinal is not directly reduced to all-*trans*-retinol. The reactions for this alternate route of all-*trans*-retinal are depicted in red. N-Ret-PE is created from the excess all-*trans*-retinal and PE, which is transported out of the disc by ABCA4 and then hydrolysed to all-*trans*-retinal to re-join the visual cycle. This figure was modified from (Liu et al., 2021) and (Molday et al., 2022) and was created using BioRender.com

1.2 ABCA4

The transmembrane protein ABCA4 is encoded by the *ABCA4* gene. This gene is comprised of 50 exons spanning 128 kb of genomic DNA, and the ABCA4 protein consists of 2273 amino acids with a molecular mass of about 250 kDa (Allikmets et al., 1997; Tsybovsky et al., 2010). When the transmembrane protein ABCA4 was first characterised, it was initially referred to as the rim protein because of its location in the rim region of the disc structures in the outer segments and incisures of rod photoreceptors (Papermaster et al., 1976). It has also previously been denoted ABCR after it was shown that the rim protein was an ABC transporter (Azarian & Travis, 1997).

As stated, the function of ABCA4 is to transport N-Ret-PE from the luminal leaflet to the cytoplasmic leaflet of the disc membrane in photoreceptors, functioning as a flippase. Once transported to the cytoplasmic leaflet, N-Ret-PE is hydrolysed into PE and all-*trans*-retinal. Subsequently, all-*trans*-retinal is reduced to all-*trans*-retinol by RDH8 and the substrate is re-entered into the visual cycle. (Tsybovsky et al., 2010). Additionally, ABCA4 has been shown to play a role in the removal of excess 11-*cis*-retinal that do not form new rhodopsin or cone opsins in the photoreceptors. 11-*cis*-retinal also forms N-Ret-PE but as an 11-*cis* isomer of that. For the clearance of this derivative, the compound must first be isomerised into its all-*trans*-isomer, allowing for the reduction of all-*trans*-retinal to all-*trans*-retinol by RDH8 (Quazi & Molday, 2014).

1.2.1 Structure

The structure of WT ABCA4 has been determined using single-molecule cryogenic electron microscopy (cryo-EM). ABCA4 consists of several domains organised in an elongated shape, stretching out of both the cytoplasmic and the intradiscal leaflet of the membrane. As depicted in Figure 1.3, the protein consists of two homologous halves, each containing an exocytoplasmic domain (ECD) that is faced towards the lumen of the discs, a transmembrane domain (TMD) that includes two extracellular α-helices (EH), and a cytoplasmic domain consisting of a nucleotide binding domain (NBD) and a regulatory domain (RD). Bound to each of the RDs are two short pinning helices (PH) (Bungert et al., 2001; Liu et al., 2021). One of the PHs, which is bound to RD2, contains the Val-Phe-Val-Asn-Phe-Ala (VFVNFA) sequence, which is crucial in the protein folding and functional activity of ABCA4 (Liu et al., 2021; Zhong et al., 2009).

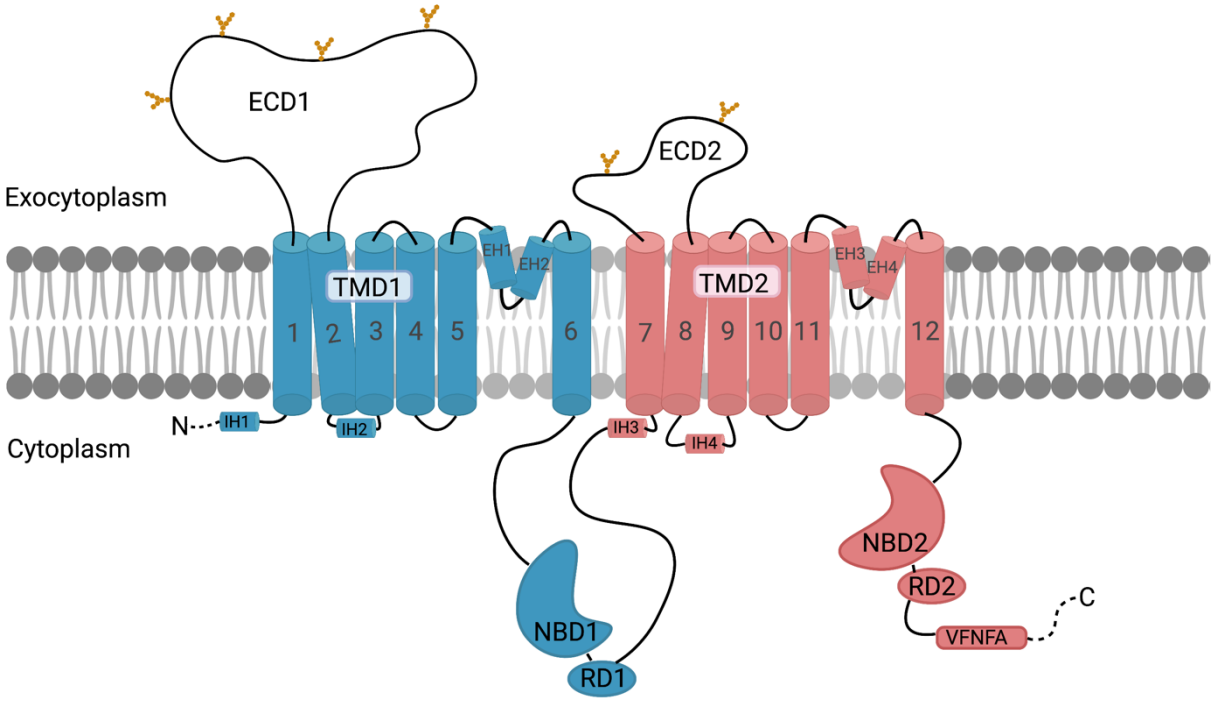

Figure 1.3: Topological diagram showing the organisation of ABCA4 in the disc membrane. The protein consists of the glycosylated ectodomains ECD1 and ECD2 faced towards the disc lumen, TMD1 and TMD2 consisting of 12 α-helices, TM1-12, in total, in addition to two extracellular α-helices each, EH1-4. NBD1 and NBD2 are bound to RD1 and RD2, respectively, facing towards the cytoplasm. Bound to RD2 is the highly conserved VFVNFA sequence. The figure was created using BioRender.com and was modified from (Curtis et al., 2020).

ABCA4 holds different conformational structures, depending on the presence of ATP and N-Ret-PE. In its resting apo-state, the two ECDs in ABCA4 are packed closely together, and create one unit with a large extended hollow interior. The TMDs, consisting of six α-helices each, numbered by convention from TM1 to TM12, adopt an outward facing configuration creating a large hydrophobic cavity between TM1, TM2, TM5 and TM7. The two NBDs in the cytoplasmic domain are kept apart, but the two RDs flanking each NBD form extensive interdomain interactions (Liu et al., 2021). The structure of ABCA4 upon substrate binding has also been determined through cryo-EM. Overall, the structure is essentially identical to the structure of apo ABCA4. The only exception is the slightly different conformation of a connecting loop between one of the transmembrane segments and ECD2 in the structure where N-Ret-PE is bound (Xie et al., 2021). However, in the presence of ATP, there is a large conformational change in ABCA4. Both the two NBDs and the TMDs are brought into close contact, the NBDs form a closed dimer, and the hydrophobic cavity is absent. The ECDs also change, positioning the hollow channel above EH3 and EH4 (Liu et al., 2021).

1.2.2 Transport mechanism

The conformational changes in ABCA4 have been used to explain the transport mechanism of N-Ret-PE from lumen to the cytoplasmic leaflet of the membrane (Figure 1.4). The hydrophobic cavity created by the two TMDs interacting with acyl chains in PE allows for a high affinity binding of N-Ret-PE (Xie et al., 2021). The transport mechanism starts when one ATP molecule binds to each of the NBDs. This results in NBD dimerization, sandwiching ATP between the NBDs, leading to a major conformational change as outlined above. The TMDs then move toward each other in a scissor-like twisting motion, leading to the collapse of the hydrophobic cavity that is bound to N-Ret-PE. This movement performed by the TMDs results in dissociation of N-Ret-PE and releases the compound to the cytoplasmic leaflet of the disc membrane (Liu et al., 2021; Molday et al., 2022).

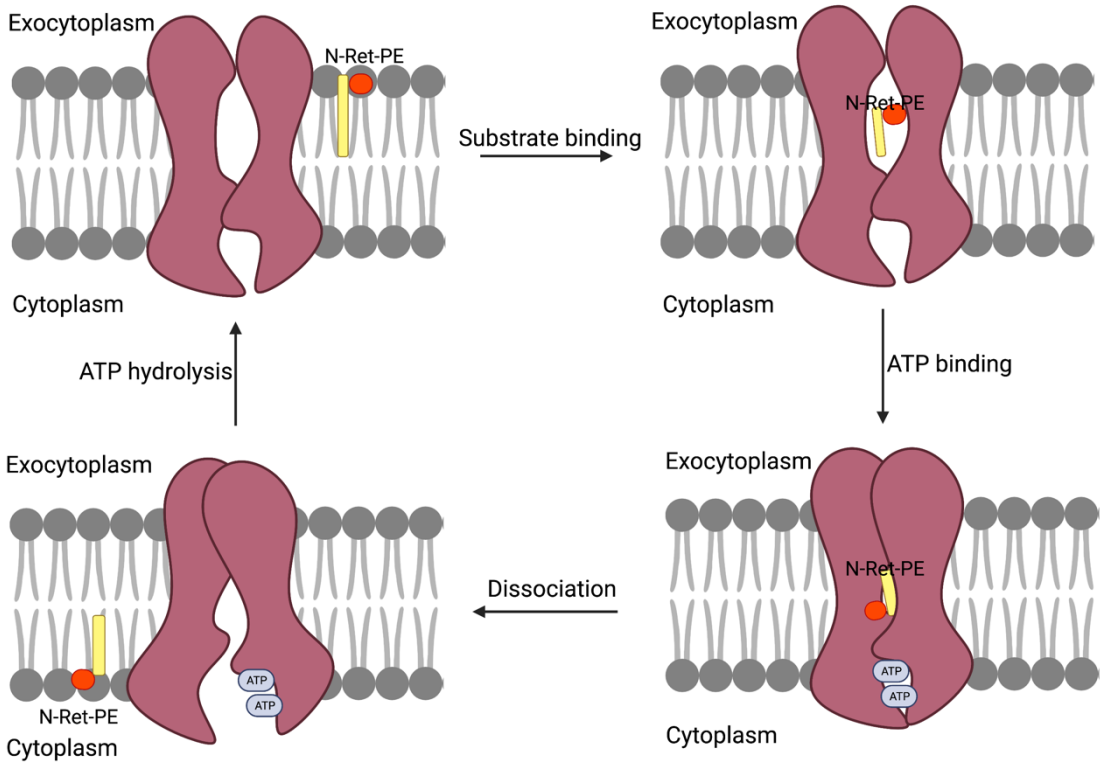

Figure 1.4: Simplistic schematic diagram of ABCA4 transporting N-Ret-PE from the luminal side through the membrane to the cytoplasmic side of the photoreceptor disc membrane. N-Ret-PE binds to the hydrophobic cavity created by the TMDs. ATP binds to the protein, creating a conformational change which releases N-Ret-PE on the cytoplasmic side of the membrane. Finally, ATP is hydrolysed, and ABCA4 converts back to its resting apo-state. The figure was created using BioRender and was modified from (Al-Khuzaei et al., 2021).

1.3 Disease-causing variants in ABCA4 and Inherited Retinal Dystrophies

1.3.1 Non-functioning ABCA4

The function and structure of ABCA4 can be affected by variants of the *ABCA4* gene. A non-functioning ABCA4 protein will lead to an accumulation of N-Ret-PE and all-*trans*-retinal in the disc membranes of photoreceptors. The accumulation of these products will induce the production of the fluorescent bis-retinoid phosphatidylethanolamine derivative A2PE in the outer segments of the photoreceptors (Ben-Shabat et al., 2002; Weng et al., 1999). When the photoreceptors are phagocytosed by RPE cells the photoreceptor outer segments are shed, and A2PE is hydrolysed by lysosomal enzymes to the pyridinium bis-retinoid A2E (Liu et al., 2000; Sakai et al., 1996; Sparrow et al., 2008). A2E cannot be further metabolised, therefore accumulates in the RPE cells, and forms a major component of lipofuscin. Lipofuscin consists of A2E and numerous other bis-retinoid compounds and has a toxic effect on RPE cells. The formation of lipofuscin therefore leads to degeneration of RPE cells. The loss of RPE cells eventually leads to the loss of photoreceptors, as these cells rely on RPE cells to recycle all-*trans*-retinal, removal of aged discs and nutrients, in addition to other functions (Molday et al., 2022; Molday & Zhang, 2010; Sparrow & Boulton, 2005; Strauss, 2005; Tsybovsky et al., 2010).

1.3.2 Inherited retinal dystrophies

Inherited retinal dystrophies (IRD) are a group of diverse genetic diseases that are characterised by degeneration of the retina, which causes progressive vision loss. The most common cause of IRDs is variants in the gene encoding ABCA4 (Holtan et al., 2020; Stone et al., 2017) with more than 1300 disease-causing variants reported to date (Chen et al., 2022; Holtan et al., 2021; Landrum et al., 2018). The severity of these mutations differs, leading to a variety of clinical phenotypes associated with the *ABCA4* gene. The group of diseases related to *ABCA4* variants can collectively be referred to as ABCA4-retinal dystrophies and include the clinical diagnoses autosomal recessive (AR) Stargardt macular dystrophy (Allikmets et al., 1997) and AR fundus flavimaculatus (Klevering et al., 2005) which have been proven to be clinically identical (Molday et al., 2022), AR cone-rod dystrophy (Cremers et al., 1998; Maugeri et al., 2000), AR generalised choriocapillaris dystrophy (Bertelsen et al., 2014) and AR pan-retinal migration patterns resembling retinitis pigmentosa (Cremers et al., 1998; Martínez-Mir et al., 1998). Some of the general characteristics of each of these variants are listed in Table 1.1

Table 1.1: General characteristics of ABCA4-retinal dystrophies

ABCA4-retinal dystrophy	General characteristics
AR Stargardt AR fundus flavimaculatus	- Bilateral central vision loss - Loss of colour vision - Central or paracentral scotoma (Regions of reduced information within the visual field) - Macular atrophy - Yellow-white fundus flecks (deposits/flecks on the interior surface of the eye, including the retina) - Night blindness, photophobia - Typically, juvenile age of onset (Fishman et al., 1999; Michaelides et al., 2003; Rotenstreich et al., 2003; Strauss et al., 2016).
AR Cone-rod dystrophy	- Bilateral central vision loss - Loss of colour vision - Central scotoma - Abnormality of retinal pigmentation - Night blindness, photophobia (Ducroq et al., 2002; Klevering et al., 2002; Maugeri et al., 2000)
AR Generalised choriocapillaris dystrophy	- Severe retinal dystrophy in addition to choriocapillaris dystrophy (Choriocapillaris: dense network of capillaries essential for supporting normal vision, supplying nutrients, and removing waste products from the RPE) - Lack of fundus flecks in early stages (Bertelsen et al., 2014)
AR pan-retinal migration patterns resembling retinitis pigmentosa	- Progressive degeneration of the retina (Cremers et al., 1998; Martínez-Mir et al., 1998)

The different disease-causing variants in the *ABCA4* gene are disrupting the ABCA4 protein function in different ways, leading to a variety of disease manifestations in patients. This is observable when it comes to clinical presentations, rates of progression, imaging, psychophysical and electrophysiological findings, and prognosis (Tanna et al., 2017).

Stargardt disease is the most common form of hereditary recessive macular dystrophies, affecting 1 in 10 000 people (Garces et al., 2018). The phenotype of Stargardt is variable, but characteristic features of the disease include the presence of yellow-white fundus flecks, macular atrophy, and sparing of the peripapillary region (the area surrounding the optic disc of the retina). These findings are present in combination with central vision loss including dyschromatopsia (loss of colour vision) and central scotoma (Tanna et al., 2017). The age of onset for this disease is variable, but most of the patients experience a loss of visual acuity in their first or second decade of life, with progressive reduction of vision throughout their life. Progression of the disease also varies, but for patients with an early onset of the disease, there is a relatively rapid progression to an advanced stage where severe vision loss is experienced

(Lambertus et al., 2015). For patients with a later onset of disease, there is typically a less severe phenotype, and a slower progression (Westeneng-van Haaften et al., 2012).

1.4 Variants of *ABCA4*

1.4.1 Classification of *ABCA4* variants

ABCA4-retinal dystrophies have an inheritance pattern that is autosomal recessive, caused by bi-allelic variants in the *ABCA4* gene (Allikmets et al., 1997). Hence, both homozygous and compound heterozygous variants of *ABCA4* can be the cause of IRDs (Cornelis et al., 2017). *ABCA4* variants can be classified by the variant effect, which includes missense, nonsense, insertions/deletions, canonical and noncanonical splice site defects and deep-intronic variants (Molday et al., 2022). To further group these variants, they are separated based on their proposed severity. Categories of severity to group the *ABCA4* variants include deleterious, severe, moderate, mild, and hypomorphic. However, this method of categorising the variants is not always precise. Because of this, severity assignments can be a difficult task, and the methods of classification must be constantly updated (Cremers et al., 2020).

1.4.2 Pathogenic mechanisms of *ABCA4* variants

Loss of function of the ABCA4 protein can be caused by many different genetic defects. Disease-causing variants will in most cases lead to the protein losing its ability to work as a transporter for N-Ret-PE. Depending on the variants, the function of the ABCA4 protein will be affected differently and vary in severity. Loss of function can be due to the absence or reduction of protein expression, protein misfolding, cellular mislocalisation, loss of key residues required for substrate transport, or problems related to ATP binding or hydrolysis. The ABCA4 protein can also be affected by a combination of some of these pathogenic mechanisms (Cornelis et al., 2017; Molday et al., 2022).

1.4.3 Characterisation of *ABCA4* variants

Methods for characterising the *ABCA4* variants include cultured cells transfected with ABCA4-encoding vectors to study the protein expression of each variant compared to WT ABCA4. The variants are studied in regard to levels of protein expression after solubilization in a mild detergent, subcellular localisation, and ATPase activity. To study the localisation of *ABCA4* variants, immunofluorescence microscopy has been performed, while the protein expression has been characterised using western blotting. The final important factor in studying the

function of these variants is to characterise both the basal and all-*trans*-retinal induced ATPase activity (Curtis et al., 2020). The use of these methods to characterise *ABCA4* variants has been important in understanding the molecular mechanism for the loss of function for the different missense variants of *ABCA4*.

Characterisation of *ABCA4* variants has shown that variants differ significantly when it comes to both the level of protein expression after solubilization, as well as their intracellular localisation (Curtis et al., 2020; Garces et al., 2018; Garces et al., 2020). Importantly, the studies showed that for variants where protein expression was above 70-80% of WT ABCA4, the immunofluorescence-stained samples generally showed a localisation that was similar to the WT protein. For WT and variants expressed at equal levels or close to WT, ABCA4 is observed in vesicular-like structures in addition to some reticular staining of the endoplasmic reticulum (ER). For the variants expressing ABCA4 at a lower level, the protein tends to almost exclusively co-localise with calnexin, predominantly showing a reticular staining pattern characteristic of ER localisation (Garces et al., 2018; Garces et al., 2020). This supports the general assumption that *ABCA4* variants where protein expression after solubilization is low, are likely misfolded and therefore retained in the ER, a characteristic that is consistent with global protein misfolding (Garces et al., 2020; Gregersen, 2006).

1.4.4 Genotype-phenotype correlations of *ABCA4* variants

Based on earlier work, genotype-phenotype association in ABCA4 was thought to entirely correlate with the residual function, if any, of ABCA4. This model of genotype-phenotype association is still valid in some cases of ABCA4-associated retinopathies. However, there is a large heterogeneity in phenotypes of ABCA4-related diseases, and a complex landscape of independent disease trajectories not only determined by the genotype (Cremers et al., 2020). More specific models are therefore needed to unravel and discuss genotype-phenotype correlations.

An important point to consider when looking at genotype-phenotype correlations is detailed knowledge about specific, well-studied variants. Knowledge about hypomorphic and modifier alleles has brought a new perspective on genetic and phenotypic heterogeneity, particularly for ABCA4-related diseases (Bauwens et al., 2019; Runhart et al., 2018; Zernant et al., 2017). An example of this type of variant is p.(Asn1868Ile), the most prominent of the hypomorphic variants (Maugeri et al., 2002; Webster et al., 2001). The mutated allele is only pathogenetically

penetrant when in *trans* with a severe *ABCA4* variant, but the phenotype has a late age of onset in addition to other distinctive clinical characteristics. When occurring in *cis* with other mutations, in addition to a severe mutation in trans, the phenotype is severe with an early age of onset, which is consistent with the general genotype effect (Zernant et al., 2017). Other important knowledge in making precise genotype-phenotype predictions is that two deleterious alleles in *ABCA4* consistently result in early onset of disease with a rapid progression to advanced disease stages (Cremers et al., 2020). These patients will experience profound visual impairment and deep, retinal-wide degeneration, and have therefore often been diagnosed with cone-rod-dystrophy or retinitis pigmentosa.

Another factor that helps in the understanding of the phenotype-genotype correlations is that the c.5882G>A, p.(Gly1961Glu) allele continuously is associated with mild disease when homozygous. For this variant, the phenotype is significantly different, depending on whether it appears homozygous or compound heterozygous (Cremers et al., 2020). Patients that harbour either p.(Gly1961Glu) or p.(Asn1868Ile) consistently exhibit milder spatiotemporal fleck patterns that never progress to the absolute confluence stage (Burke et al., 2014). These two variants additionally appear to present with individual morphology of distinct flecks that are larger in size and have a well-defined shape. The p.(Gly1961Glu) allele appears to act as a clinically dominant allele, as the phenotype bull's eye maculopathy is normally present, regardless of the allele in trans (Cella et al., 2009).

1.5 Aim of the thesis

A patient under clinical investigation at Haukeland University Hospital was diagnosed with early onset severe ABCA4-retinopathy caused by homozygosity for a doubly mutated allele consisting of two homozygous variants: c.5882G>A, p.(Gly1961Glu) and c.634C>T p.(Arg212Cys). Due to the clinical severity and early onset of disease, we hypothesised that the two variants had a synergistic or at least additive effect, compared to the single variants. The aim of the thesis was therefore to characterise these specific mutations of ABCA4 as single and double mutations. The characterisation was performed by investigating mRNA and protein expression levels of the variants, as well as their intracellular localisation, compared to WT ABCA4. Additionally, molecular modelling of the impact of the mutations on the 3D-model of the protein was investigated.

2. Materials

Table 2.1: Reagents and kits used for site-directed mutagenesis and plasmid purification

Product	Manufacturer	Catalogue number
XL10-Gold ultracompetent cells	Agilent Technologies	200314
QuikChange II XL Site-Directed Mutagenesis Kit	Agilent Technologies	200522-5
imMedia Amp Agar	Invitrogen	45-0034
imMedia Amp Liquid	Invitrogen	45-0035
LB Broth tablets		L7275
S.O.C. Medium	Invitrogen	15544-034
QIAprep Spin Miniprep Kit	QIAGEN	12263
QIAfilter Plasmid Maxi Kit	QIAGEN	12262
MAX Efficiency DH5α competent cells	Invitrogen	18258012
Ampicillin, Sodium Salt	Millipore	171254-5GM
B-Mercaptoethanol		

Table 2.2: Primers used for site-directed mutagenesis

Variant	Direction	Sequence 5´ to 3´
ABCA4 c.634C>T	Forward	GAGGCCCTCCTGGAG**T**GCTTCATCATCTTCA
ABCA4 c.634C>T	Reverse	TGAAGATGATGAAGC**A**CTCCAGGAGGGCCTC
ABCA4 c.5882G>A	Forward	GACAGGCTGTGTGTCG**A**AGTTCGCCCTGGAGAG
ABCA4 c.5882G>A	Reverse	CTCTCCAGGGGCGAACT**T**CGACACACAGCCTGTC

Table 2.3: Restriction mapping

Product	Manufacturer	Catalogue number
NheI	Thermo Scientific	ER0971
NotI	Thermo Scientific	ER0595
Elite 2-in-1 Agarose Tablets	ProteinArk	PAL-E-2in1-100
Quick-Load 100 bp DNA Ladder	New England BioLabs	NO551S
Gel Loading Dye, Purple (6X)	New England BioLabs	B7025S
Tris-Borate-EDTA (TBE) Buffer	-	-

Table 2.4: Reagents used for Sanger sequencing

Product	Manufacturer	Catalogue number
Amplitaq Gold 360 Master Mix	Applied Biosystems	438790
illustra ExoProStar 1-step	Cyvita	US79050
BigDye Terminator v1.1 Ready reaction mix	Applied Biosystems	4337452
BigDye 5x Sequencing buffer	Applied Biosystems	4336699

Table 2.5: Primers used for Sanger sequencing of ABCA4 cDNA

Primer name No. refers to c.DNA pos. in NM_000350	Direction	Sequence 5´to 3´
p. 2-25, pair 0	Forward	TGGGCTTCGTGAGACAGATACAGC
p. 423-444 pair 0	Reverse	TCCTGCAATTCTCTCCGGGTGA
p. 346-367, pair 1	Forward	GCACCAGAGAGCCAGCACCTTG
p. 954-975 pair 1	Reverse	GCCACACAGGAGGTCAGACAGG
p. 863-884, pair 2	Forward	TCCATCGGCCGAGTATGCAGGA
p. 1442-1463, pair 2	Reverse	TCCCGAGGGCCCTTGTAGAGGA
p. 1346-1369 pair 3	Forward	ACATGATCAGAGATACCCTGGGGA
p. 1946-1968, pair 3	Reverse	AGGGAAACAGCGGTTCAGGATGA
p. 1855-1876, pair 4	Forward	ATCACAAGGAGCCAGGTGCAGG
p. 2434-2455, pair 4	Reverse	GCCCCAGGCCTTGCTCTTCAAA
p. 2321-2342, pair 5	Forward	TGCCACACATCCTGTGCTTCGC
p. 2921-2942, pair 5	Reverse	GGCAACAGACCCGTCAGGATGG
p. 2829-2850, pair 6	Forward	GCCAGCTGTGGACCGTCTGAAC
p. 3419-3440, pair 6	Reverse	AGGAAGAGTGGGGTGCCTGAGC
p. 3348-3369, pair 7	Forward	CACTCACCACATGGACGAGGCC
p. 3884-3905, pair 7	Reverse	GGGTGTCGGGGGTTGACGTTTT
p. 3845-3866, pair 8.2	Forward	TCTGACACTCCCCTGGAAGAGA
p. 4395-4417, pair 8.2	Reverse	TGCAGGATGGTGAAGGGTTGACC
p. 4344-4365, pair 9	Forward	GTGGCTTCCGGAGTACCCCTGT
p. 4890-4911, pair 9	Reverse	GGCGTTGTGGGCCACATTGAGA
p. 4831-4855, pair 10	Forward	ACTGAAGACAACATTAAGGTGTGGT
p. 5402-5423, pair 10	Reverse	GCACTGCTGTTGATGCCGATGA
p. 5300-5321, pair 11	Forward	TCCTGCTGTATGGATGGGCGGT
p. 5879-5900, pair 11	Reverse	CACTCTCCAGGGCGAACTCCGA
p. 5834-5856, pair 12	Forward	AGATTTATCCAGGCACCTCCAGC
p. 6408-6429, pair 12	Reverse	CATGATGGCCAGCCGGGTACAC
p. 6317-6338, pair 13	Forward	GCCGCATGCTGTGGAACGTCAT
p. 6791-6812, pair 13	Reverse	GCTTGTCGACTGGCTCCAGCAG
p.586-601, pCEP	Forward	AGAGCTCGTTTAGTGAACCG
p.7518-7537, EBV	Reverse	GTGGTTTGTCCAAACTCATC

Table 2.6: Cell culture

Product	Manufacturer	Catalogue number
Dulbecco's Modified Eagle Serum (DMEM) + GlutaMAX	gibco	2393638
Fetal Bovine Serum (FBS)	Sigma-Aldrich	F7524
Penicillin Streptomycin (PenStrep)	Sigma-Aldrich	P4333
Sodium Pyruvate (100mM)	gibco	11360-070
MEM NEAA (100X)	gibco	11140-036
Dulbecco's Phosohate Buffered Saline (PBS)	Sigma-Aldrich	D8537
0.05% Trypsin-EDTA (1X)	gibco	25300-054
Geneticin Selective Antibiotic (50 mg/mL)	gibco	10131-027
jetPRIME	Polyplus transfection	114-15
HEK293ft cells	Invitrogen	R700-07
HELA cells	ATCC	CCL-2
MycoStrip 100 – Mycoplasma Detection kit	Invivogen	rep-mys-100

Table 2.7: SDS-PAGE and Western Blot

Product	Manufacturer	Catalogue number
cOmplete EDTA-free Protease inhibitor Coctail	Roche	11836170001
Pierce BCA Protein Assay Kit - Reducing Agent Compatible	Thermo Scientific	23250
Methanol for analysis EMSURE ACS,ISO, Reag. Ph Eur	Millipore	106009
Mini-PROTEAN TGX Stain-Free Gels (4-20%, 12 well comb)	BIO-RAD	4568095
4x Laemmli Sample Buffer	BIO-RAD	1610747
10x Tris/Glycine/SDS Buffer	BIO-RAD	1610772
Precision Plus Protein Standards All Blue	BIO-RAD	1610373
Precision Plus Protein unstained standards	BIO-RAD	1610363
Trans-Blot Turbo RTA Transfer Kit, LF PVDF	BIO-RAD	1704274
EveryBlot Blocking buffer	BIO-RAD	12012020
DTT (100mM)		
Anti-Rho1D4 Mouse Monoclonal Antibody	Merck	MAB5356
Beta-actin (C4) mouse monoclonal (200µg/mL)	Santa Cruz Biotechnology	sc-47778
m-IgGk BP-HRP	Santa Cruz Biotechnology	sc 516102
Precision Protein Strep-Tactin-HRP Conjugate	BIO-RAD	1610380
PBS Tablets	gibco	18912014
Tween20	Merck	8.22184.0500
Clarity Western ECL Substrate	BIO-RAD	170-5061

Table 2.8: RNA purification and quantification

Product	Manufacturer	Catalogue number
Rneasy Mini Kit	QIAGEN	74104/74106
RNase-Free DNase Set	QIAGEN	79254
RNA ScreenTape Sample Buffer	Agilent Technologies	5067-5577
RNA ScreenTape Ladder	Agilent Technologies	5067-5578
RNA ScreenTape	Agilent Technologies	5067-5576

Table 2.9: Taqman-assay master mix and probes

Product	Manufacturer	Catalogue number
SuperScript IV VILO Master Mix	Invitrogen	11766050
TaqMan 2X Universal PCR-Mix	Applied Biosystems	4304437
Actin Beta (ACTB, exon 2-3)	Applied Biosystems	Hs01060665_g1
beta-2-microglobulin (B2M, exon 1-2)	Applied Biosystems	Hs00187842_m1
ATP binding cassette subfamily A member 4 (ABCA4, exon 4-5)	Applied Biosystems	Hs00979595_m1

Table 2.10: Immunofluorescence

Product	Manufacturer	Catalogue number
Normal Goat Serum	Invitrogen	10000C
Prolong Diamond Antifade Mountant with DAPI	Invitrogen	P36966
0.1% Triton X-100	Sigma-Aldrich	T8787
Anti-Rho1D4 Mouse Monoclonal Antibody	Merck	MAB5356
Calnexin Rabbit Monoclonal Antibody	Cell Signalling Technologies	C5C9
Goat anti mouse IgG (H+L), Alexa Fluor 594	Invitrogen	A-11012
Goat anti-rabbit IgG (H+L), Alexa Fluor 488	Invitrogen	A11070

Table 2.11: Instruments

Instrument	Supplier
NanoDrop One Microvolume UV-Vis Specrophotometer	Thermo Scientific
3730xl DNA Analyzer 96-Capillary Array	Applied Biosystems
Mini-Protean Tetra system	BIO-RAD
Trans-Blot Turbo transfer system	BIO-RAD
ChemiDoc MP Imaging system	BIO-RAD
Veriti 96-Well Fast Thermal Cycler	Applied Biosystems
MWG Sirius HT	MWG Biotech
4200 TapeStation System	Agilent
7900HT Fast Real-Time PCR System	Applied Biosystems
Leica SP8-STED confocal microscope	Leica Microsystems

Table 2.12: Software

Software	Developer	Version
PyMOL	Schrödinger	2.5.4
SeqScape	Applied biosystems	2.5
Gen5 Microplate Reader	BioTek	2.06
ImageLab	BIO-RAD	6.1
BioRender.com	app.biorender.com	-
PubMed	National Center for Biotechnology Information	-
Sequence Detection System	Applied biosystems	2.4
Excel	Microsoft	16.54
Word	Microsoft	16.54
PowerPoint	Microsoft	16.54

3. Methods

3.1 Site-directed mutagenesis

To create the missense *ABCA4*-variants that were studied in this project, site-directed mutagenesis was performed using the QuikChange II XL Site-Directed Mutagenesis Kit (Agilent), in accordance with the protocol of the manufacturer. The single mutations were created using the wild-type ABCA4 (WT) plasmid (pCEP4_ABCA4) (Zhong et al., 2009) as the template, in combination with specific primers that contained the desired mutation. The expression vector pCEP4-ABCA4 contains the cDNA for human ABCA4 (NM_000350) fused to a 1D4 tag (amino acid sequence TETSQVAPA, derived from bovine rhodopsin (MacKenzie et al., 1984)) at the C-terminus (see supplementary Figure 7.1 for vector map). To create the double mutation, a plasmid containing the Gly1961Glu mutation was used as the template in combination with primers containing the Arg212Cys mutation.

The site-directed mutagenesis reactions were prepared by mixing 5 µL of 10x Reaction buffer, 100 ng of the plasmid, 1.3-2.0 µL of both the forward and the reverse primer (10µM), 1 µL of deoxynucleoside triphosphate (dNTP) mix, 3 µL of QuikSolution Reagent, 1 µL of PfuUltra High Fidelity (HF) DNA Polymerase, and MilliQ H_2O to a final volume of 50 µL. This reaction was run using the thermal cycling program as indicated in Table 3.1.

Table 3.1: Thermal cycling-program used for site-directed mutagenesis.

Cycles	Temperature (ºC)	Time
1	95	1 min 30 sec
18	95	60 sec
	60	50 sec
	68	20 min
1	68	7 min

After the thermal cycling, the samples were placed on ice for 2 minutes and 1 µL of DpnI restriction enzyme (10 U/µL) was added to all samples. Thereafter, the samples were incubated at 37ºC for 1 h.

3.2 Transformation

For transformation of the mutated plasmids, XL10-Gold ultracompetent cells were used. The ultracompetent cells were thawed on ice, and 45 µL were aliquoted into prechilled polypropylene round-bottom tubes and then mixed with 2 µL β-Merceptoethanol. This mixture

was incubated on ice for 10 min, being gently swirled every 2 min. 2 µL of the site-directed mutagenesis products was added to the cell mixtures, swirled, and incubated on ice for 30 min. Thereafter, the samples were heat-shocked in a 42 ºC water bath for 30 sec and then placed back on ice for 2 min. 0.5 µL of Super Optimal Broth (S.O.C) medium, pre-heated to 42 ºC, was added to each sample and incubated for 1 h at 37 ºC with continuous shaking at 225 revolutions per minute (rpm). After this, samples were plated onto Luria Bertani (LB) agar plates containing ampicillin (100 µg/mL), incubated overnight (ON) at 37 ºC, and then stored at 4 ºC.

Single colonies were picked from the agar plates and grown in separate containers with 3 mL LB medium containing ampicillin. This mix was incubated ON at 37 ºC with continuous shaking at 225 rpm.

3.3 Plasmid DNA purification using the QIAprep Spin Miniprep Kit

To purify the plasmid DNA from the overnight cultures, the samples were transferred to spin columns from the QIAprep Spin Miniprep Kit (QIAGEN). The purification was carried out as described in the protocol provided by the manufacturer.

3.4 DNA- and RNA-concentration measurements using NanoDrop

To estimate DNA and RNA-concentrations, samples were analysed using a NanoDrop One Microvolume UV-Vis Spectrophotometer. The absorbance of each sample was measured at 260 nm. To ensure the purity of DNA and RNA, the absorbance was also measured at 230 and 280 nm, and the ratios of 260/280 nm and 260/230 nm were assessed, respectively. A 260/280 absorbance ratio of about 1.8 is considered pure for DNA while an absorbance ratio of about 2.0 is considered pure for RNA. For the 260/230 absorbance ratio, a value of 2.0-2.2 is accepted as pure for both nucleic acids.

3.5 Restriction mapping

To ensure insertion of the ABCA4 insert after maxiprep, restriction mapping was performed. Enzymes used in the restriction mapping of the ABCA4 plasmids were NheI (10 U/µL) and NotI (10 U/µL) (Thermo Scientific). First, a reaction mix with NheI was prepared containing 2 µL of 10x Tango-Buffer, 1 µL of NheI, 0.2-6.0 µL of the plasmid DNA sample (1000 ng) and 11.0-15.8 µL MilliQ H_2O.

Using a thermocycler, the samples were digested at 37 ºC for 90 min and inactivated at 65 ºC for 20 min. After digestion and inactivation with NheI, the buffer concentration was doubled by adding 2.3 µL of 10x tango buffer, followed by the addition of 1 µL NotI. The samples were then digested with NotI at 37 ºC for 90 min and inactivated at 80 ºC for 20 min. 3 µL of each sample was transferred to another tube before doubling the buffer concentration and adding NotI, to use as controls for the function of the enzymes. All the prepared samples were mixed with Gel Loading Dye, Purple 6X (New England BioLabs) and loaded onto a 0.5% agarose gel made using Elite 2-in-1 Agarose tablets with Quick-Load 100 bp DNA Ladder (New England BioLabs). The gel was run at 100 V until the tracking dye had reached the end of the gel.

3.6 Sanger sequencing

To confirm the site-directed mutagenesis, the samples were sequenced using Sanger sequencing. For this study, the samples were first confirmed in miniprep samples using primers covering the area in which the mutagenesis occurred. Then, once the samples had been maxiprepped, the whole insert was sequenced using 15 different primer pairs.

Preparing the samples for Sanger sequencing included a polymerase chain reaction (PCR) and purification of the PCR-product. Firstly, a PCR was performed using specific reverse and forward primers (Table 2.5). For each sample, a mix was prepared containing 10 µL AmpliTaq Gold 360 master mix, 2 µL of each primer (5 µM), 5 µL MilliQ H_2O and 1 µL plasmid DNA (10-100 ng/µL). The PCR was then run as presented in Table 3.2.

Table 3.2: PCR-program used to prepare samples for Sanger sequencing

Cycles	Temperature (ºC)	Time
1	94	10 min
35	94	20 sec
	58	20 sec
	72	30 sec
1	72	7 min

Unincorporated nucleotides and primers were removed using Illustra ExoStar 1-step, before continuing to sequencing. 2 µL of Illustra ExoStar 1-step was mixed with 5 µL of the PCR-product and incubated for 15 min at 37 ºC. The enzymes were inactivated by 15 min incubation at 80ºC.

For the sequencing reaction, a mix was prepared containing 1.0 µL of BigDye Terminator v1.1 Ready reaction mix**,** 2.0 µL BigDye 5x Sequencing Buffer, 1.0 µL of either the forward or reverse primer (5µM) used for the initial thermal cycling, 1.0 µL of the template, and 5.0 µL MilliQ H_2O. Then, cycle sequencing was carried out as presented in Table 3.3.

Table 3.3: Thermal cycling program used for the Sanger sequencing reaction

Cycles	Temperature (ºC)	Time
1	96	1 min
25	96	10 sec
	58	5 sec
	60	4 min

The samples were stored at -20 ºC and sequenced through capillary electrophoresis using the 3730 XL DNA Analyser.

3.7 Increasing the quantity of the DNA plasmids

After confirmed site-directed mutagenesis, the sample quantity was increased using QIAfilter Plasmid Maxi Kit (QIAGEN). To achieve this, transformation was performed using the purified miniprep samples and MAX Efficiency DH5α competent cells.

The competent cells were thawed on ice, and 100 µL were aliquoted into chilled polypropylene round-bottom tubes. 1 µL of the plasmid was added to the cells, after which the samples were incubated on ice for 30 min. Following this, the samples were heat-shocked for 45 sec at 42 ºC and then placed on ice for 2 min. 0.9 mL S.O.C medium was then added, and the samples were incubated at 37 ºC for 1 h with continuous shaking at 225 rpm. After this, the samples were plated onto LB plates with ampicillin and incubated ON at 37 ºC. Single colonies were picked from the agar plates and grown in separate containers with 5 mL LB medium containing ampicillin. This mix was incubated for 6-8 h at 37ºC with continuous shaking at 225 rpm. Thereafter, the samples were purified using the QIAfilter Plasmid Maxi Kit (QIAGEN), following the protocol provided by the manufacturer.

3.8 Cell culture work

The cell lines HEK293FT and HeLa were used for cell experiments in this study. The HEK293FT cell line is a fast growing, highly transfectable clonal isolate derived from human

embryonic kidney cells transformed with SV40 large T antigen. The HeLa cell line is derived from a cervical cancer tumour. Both cell lines were cultured in high glucose Dulbecco's Modified Eagle Medium (DMEM) + GlutaMAX with 4.5 g/L D-Glucose and Pyruvate. This medium was supplemented with 10% Fetal Bovine Serum (FBS), 1 mM Sodium Pyruvate, 0.1 mM Minimum Essential Medium Non-Essential Amino Acids (MEM NEAA), 1% Pen-Strep and 6 mM L-Glutamine. Additionally, the medium used for culturing the HEK293FT cells was filtered and supplemented with 500 µg/mL of the selective antibiotic Geneticin.

For both cell lines, cells were stored in liquid nitrogen. When thawing cells, the tube was placed in a 37 ºC water bath until only a small part of cells remained frozen. The cells were then transferred to a 15 mL tube containing supplemented DMEM without Geneticin. The tube was centrifuged at 300 g for 5 min, the supernatant was discarded, and the cells were resuspended in medium. The cells were then transferred to a T-25 cm^2 flask and incubated ON at 37 ºC with 5% CO_2. For the HEK293FT cells, the medium was aspirated and replaced by medium containing 500 µg/mL Geneticin after 24 h.

After the primary growth in T-25 cm^2-flasks, the cells were kept in T-75 cm^2 flasks. The cells were split at around 80% confluency, for both cell lines. The medium was removed, the cells were washed with phosphate buffered saline (PBS), and 0.05% trypsin at a volume corresponding to flask size was added. The flask was placed in 37 ºC with 5% CO_2 for approximately 5 min to detach the cells from the flask. Once the cells loosened, fresh supplemented DMEM was added to the flask. The cells were then diluted at either 1:10, 1:15 or 1:20, added to a fresh flask and placed in 37 ºC with 5% CO_2.

For transient transfection reactions, the cells were seeded into either 6-well plates ($5*10^5$ cells/well) or 12-well plates ($8*10^4$ cells/well). Counting of the cells was carried out using the Scepter 2.0 Handheld Automated Cell Counter (Millipore), using a 60 µm Scepter Sensor for both cell lines.

3.9 Mycoplasma testing

To ensure that there was no contamination of the cells that were used in experiments, the mycoplasma test MycoStrip 100 (Invivogen) was used. 1 mL of the cell culture supernatant was transferred to a 1.5 mL microcentrifuge tube and centrifuged at 16 000 g for 5 min. After

centrifugation, the supernatant was removed, and 500 µL of sterile PBS was added to the tube. After this, 5 µL of both Reaction Buffer and the prepared sample were mixed. This sample was incubated at 40 ºC for 40 min. After incubation, 200 µL of Migration Buffer was added to the mixture. A detection strip was then placed in the sample tube, and the result was read after 2-5 minutes. The same process was performed using the positive control provided in the kit and for a negative control consisting of sterile PBS.

3.10 Transient transfection of HeLa and HEK293ft cells

HeLa cells and HEK293ft cells were seeded into either 6-well plates ($5*10^5$ cells/well) or 12-well plates ($8*10^4$ cells/well) 24 h before transfection. At 60-80 % confluency, cells were transfected using the jetPRIME transfection reagent (Polyplus-transfection). DNA mixes with the jetPRIME reagent and buffer were made for each well. When using 6-well plates, 3 µg DNA was diluted in 200 µL of the provided buffer, which was then vortexed for 10 sec. 9 µL jetPRIME reagent was then added, the samples were vortexed for 1 sec and then incubated for 10 min. For 12-well plates, 1.2 µg DNA was diluted in 75 µL of the buffer, and 3.6 µL jetPRIME reagent was added before vortexing and incubation. The DNA mix was added throughout the well by pipette. The cells were then incubated for 24 h at 37 ºC with 5% CO_2, changing the media 4 h after adding the transfection mix.

After 24 h, the transfected cells were harvested. Media was aspirated and ice-cold PBS was used to wash the cells twice. The cells were removed from the wells and transferred into 1.5 mL tubes. The samples were then centrifuged for 5 min at 3500 g and 4 ºC and the supernatant was removed by suction.

3.11 Western Blotting to quantify relative protein concentration

To quantify the relative concentration of ABCA4 protein in samples transfected with WT ABCA4, empty vector (EV) and the mutated variants, western blotting was performed. Western blot analysis was carried out in three biological replicates, with two technical replicates for every sample.

3.11.1 Cell lysis

The cell pellet containing transfected cells was resuspended in 20 µL resuspension buffer (50 mM HEPES pH 7.5, 150 mM NaCl, 5 mM MgCl2, 10% Glycerol, 1 mM DTT, 1X Protease

Inhibitor) and then solubilized in 125 µL solubilization buffer (20 mM CHAPS, 50 mM HEPES pH 7.5, 150 mM NaCl, 5 mM MgCl2, 10% Glycerol, 1 mM DTT, 1X Protease Inhibitor). The samples were then incubated for 40 min at 4 ºC and centrifuged at 100 000 g for 10 min. The supernatant containing the cell lysate was collected and stored at -80 ºC.

3.11.2 Quantification of total protein concentration

For equal protein loading onto the western blot, the total protein concentration of the cell lysates was quantified using the Pierce BCA Protein Assay Kit - Reducing Agent Compatible (Thermo Scientific).

A bovine serum albumin (BSA) standard curve was created by diluting the provided BSA ampule in the solubilization buffer as stated in the protocol, with a series of dilutions with concentrations of 2000, 1500, 1000, 750, 500, 250 and 125 µg/mL. To limit the effect that the reducing agent DTT may have on the results, a standard blank not containing DTT was used in addition to the sample blank. The sample blank consisted of solubilization buffer, and the standard blank was made the same way as the solubilization buffer, without DTT.

The samples were prepared in a 96-well plate, and the assay was performed as described in the protocol for the microplate kit. The absorbance of all samples was measured at 562 nm using an MWG Sirius HT plate reader and further analysed using the Gen5 2.06 software.

3.11.3 SDS-PAGE

Sodium dodecyl sulphate-polyacrylamide gel electrophoresis (SDS-PAGE) was run using 4–20% Mini-PROTEAN TGX Precast Protein Gels (Bio-Rad). Depending on the results from the total protein quantification, 5-20 µg total protein was loaded onto the gel. The cell lysate samples were mixed with 4.8 µL 4x Laemmli Sample Buffer and 4 µL DTT (100mM), which was then added to the gel. Precision Plus Protein All Blue Prestained Protein Standards and Precision Plus Protein unstained standards (BIO-RAD) were used as ladders. The gel was then run for 1 h and 10 min at 150 V with 1x TRIS/Glycine/SDS Buffer.

3.11.4 Immunoblotting

The gel from the SDS-PAGE was transferred to a low fluorescence polyvinylidene difluoride (LF PVDF) membrane using the semi-dry western blot system Trans-Blot Turbo (BIO-RAD).

The membrane was placed in methanol (99.9%) for five minutes and then moved to transfer buffer. A sandwich stack was then created in the cassette consisting of an anode plate and a cathode plate. Firstly, a transfer stack from the Trans-Blot Turbo RTA Transfer Kit that had been wet in transfer buffer was placed into the cassette, adding the membrane on top followed by the gel and finally another wet transfer stack. The cassette was run for 10 min at 2.5 A and 25 V. After completed immunoblotting, the membrane was imaged using the ChemiDoc MP Imaging system (BIO-RAD). This image was used for normalisation when quantifying the relative protein concentration after antibody incubation in the Bio-Rad Image Lab software.

3.11.5 Antibody incubation

For the identification of the ABCA4 protein, the membrane was incubated with mouse antibodies targeting the rhodopsin-derived 1D4 tag expressed by the ABCA4 expression vector. Additionally, an antibody against β-actin (C4) was included to function both as a loading control and to be used for normalisation.

To detect ABCA4 protein bands, the membrane was incubated with anti-Rho1D4 mouse monoclonal antibody (1:500) and anti-β-actin mouse monoclonal antibody (1:2000). The antibodies were mixed in EveryBlot blocking buffer. The membrane was labelled ON at 4 ºC. The membrane was then washed for 4x5 min in PBS with 0.05% Tween20. A secondary antibody mix consisting of a 1:5000 dilution of mouse IgG kappa binding protein (m-IgGK BP) conjugated to Horseradish Peroxidase (HRP) and a 1:5000 dilution of Precision Protein StrepTactin-HRP (BIO-RAD) conjugate in EveryBlot blocking buffer was made. The membrane was incubated in the secondary antibody mix for 1 h at room temperature (RT). After secondary antibody incubation, the membrane was washed using 0.05% Tween20 in PBS 4x5 min.

To visualize the targeted protein bands, the membrane was developed using the Clarity Western ECL Substrate. The two provided reagents were mixed 1:1 and pipetted onto the membrane. The membrane was then incubated for 5 min at RT. After incubation, the chemiluminescence of the membrane was imaged using the ChemiDoc MP Imaging System. To quantify the relative protein concentration, the Bio-Rad Image Lab Software version 6.1 was used.

3.12 RNA quantification through qPCR

qPCR was performed to quantify mRNA expression levels of ABCA4 in HEK293ft cells after transfection. The RNA quantification process was carried out in three biological replicates, with two technical replicates of every sample.

3.12.1 RNA-purification

RNA was purified from the transfected cell samples using the RNeasy Mini Kit (QIAGEN), in accordance with the manufacturer's protocol. To ensure that there was no DNA left in the samples, a DNase digestion step was included in the purification process. The concentration of RNA after purification was measured using NanoDrop as described in section 3.4.

To determine the quality and integrity of the isolated RNA, an RNA Screentape assay, using the Agilent 4200 TapeStation system, was performed as described in the protocol. The RNA integrity number (RIN) value was assessed and considered optimal at a value of 10.

3.12.2 cDNA synthesis

cDNA was synthesized from the RNA samples using SuperScript IV VILO Master Mix with ezDNase enzyme (Invitrogen). The reverse transcriptase reaction was carried out as described in the provided protocol. The cDNA samples were stored at -20 ºC.

3.12.3 Real-time PCR using TaqMan-assay

To quantify the expression of ABCA4, real-time PCR (qPCR) was performed using a TaqMan-assay. In this assay, reactions were prepared in triplicates using probes directed towards ABCA4, as well as the reference genes ACTB and B2M. Mixes were prepared for each triplicate containing 15 µL TaqMan 2X Universal PCR Master Mix, 1.5 µL probe (20x) and 10.5 µL MilliQ water. 9 µL of the reaction mix was pipetted into each well in a 384-well plate, and 1 µL of the template cDNA samples was added in triplicates.

The qPCR was performed and run using the 7900HT Fast Real-Time PCR system (Applied Biosystems) using the PCR program presented in Table 3.4.

Table 3.4: qPCR-program used to quantify RNA-concentration

Cycles	Temperature (ºC)	Time
1	50	2 min
1	95	10 min
40	95	15 sec
	60	1 min

3.13 Statistical analysis of the results from the protein expression and qPCR TaqMan assay

Normalisation and relative gene expression of the Ct-values from the qPCR were calculated using the average Ct-values of the triplicates. The $2^{-\Delta\Delta Ct}$ -value was calculated by finding the ΔCt-value by subtracting the mean Ct-value of either reference gene from the mean Ct-value of ABCA4. Thereafter the ΔΔCt-value was calculated by subtracting the Ct-value of the control sample.

Student's t-test was used to examine if the differences in both the variants' relative protein expression and gene expression levels were statistically different from the WT. A two-tailed t-test assuming unequal variances was used, where a p-value < 0.05 was considered significant.

3.14 Immunofluorescence

To study the localisation of the ABCA4-mutants compared to WT ABCA4 protein, HeLa cells were transfected and stained with immunofluorescent antibodies.

To start the process of creating immunofluorescent ABCA4 proteins, coverslips were placed into 12-well plates, and covered with ethanol for 5 min. The ethanol was then removed, and the coverslips were washed with 1 mL PBS. PBS was removed and $8*10^4$ HeLa cells were seeded to each well in 1 mL medium and incubated ON. The cells were then transfected using the jetPRIME protocol as described in 3.10. 24 h post transfection, the media was removed, and the cells were washed with 1 mL PBS that was pre-heated to 37 ºC. The cells were then fixed in 500 µL of 4% paraformaldehyde (PFA) solution in 0.2 M Phosphate Buffer (PB) for 15 min. The PFA was removed, and the cells were washed in 0.2 M PB 3x5 min while shaking at RT.

After washing, the cells were blocked and permeabilized using 500 µL 0.1% Triton X-100 and 10% Goat Serum in PB for 30 min at RT. 50 µL of the primary antibodies anti-Rho1D4 mouse monoclonal antibody and anti-calnexin rabbit monoclonal antibody in dilutions of 1:100 in

labelling buffer (3% Goat serum, 0.1% Trition X-100) was added to each well. The samples were incubated in the primary antibody mix for 2 h at RT. After incubation, the samples were washed in PB 3x10 min with shaking. The secondary antibody mix consisted of 1:100 dilutions of Goat anti-mouse, Alexa Fluor 594 and Goat anti-rabbit, Alexa Fluor 488. 50 µL of this mix was added to each well and incubated for 1 h at RT in the dark. Next, the cells were washed in PB 3x10 min in the dark at RT.

After washing, the coverslips were mounted onto glass slides with one drop of the mounting solution ProLong Diamond Antifade Mountant with 4′,6-diamidino-2-phenylindole (DAPI) (Invitrogen). The slides were left to harden overnight at RT, and then stored at -20 ºC. The immunofluorescent cells were then viewed and imaged using the Leica SP8-STED confocal microscope.

3.15 Theoretical molecular modelling of *ABCA4* variants

The theoretical consequences of the missense variants p.(Gly1961Glu) and p.(Arg212Cys) were investigated using molecular modelling of an AI-generated structure of the complete ABCA4 protein (Jumper et al., 2021; Varadi et al., 2022). The predicted structure of WT ABCA4 was downloaded as a PDB file from Alphafold2 and investigated using PyMol, where *in silico* site-directed mutagenesis was performed to study possible changes in the protein as a consequence of p(Gly1961Glu) and p.(Arg212Cys).

4. Results

4.1 Clinical characterisation of the patient at Haukeland University Hospital

A patient under investigation at the Department of Ophthalmology, Haukeland University Hospital was found to be homozygous for two pathogenic variants of *ABCA4*. The variants, c.5882G>A p.(Gly1961Glu) and c.634C>T p.(Arg212Cys), were detected by sequencing of the ABCA4 gene at the Department of Medical Genetics. The phenotype of the patient was characterised as severe, as he experienced a rapidly reduced visual acuity from the age of 11. The best corrected visual acuity was found to be 0.15 for the right eye and 0.2 for the left eye, where 1.0 represents normal vision. The patient also developed red-green colour deficit at the age of 13. In addition to this, bilateral macular atrophy was found, but the patient did not display any pallor of the optic disc. These findings are presented in Figure 4.1. Additionally, a full field electroretinogram showed that the patient had severely reduced cone function, but a normal response for rod function.

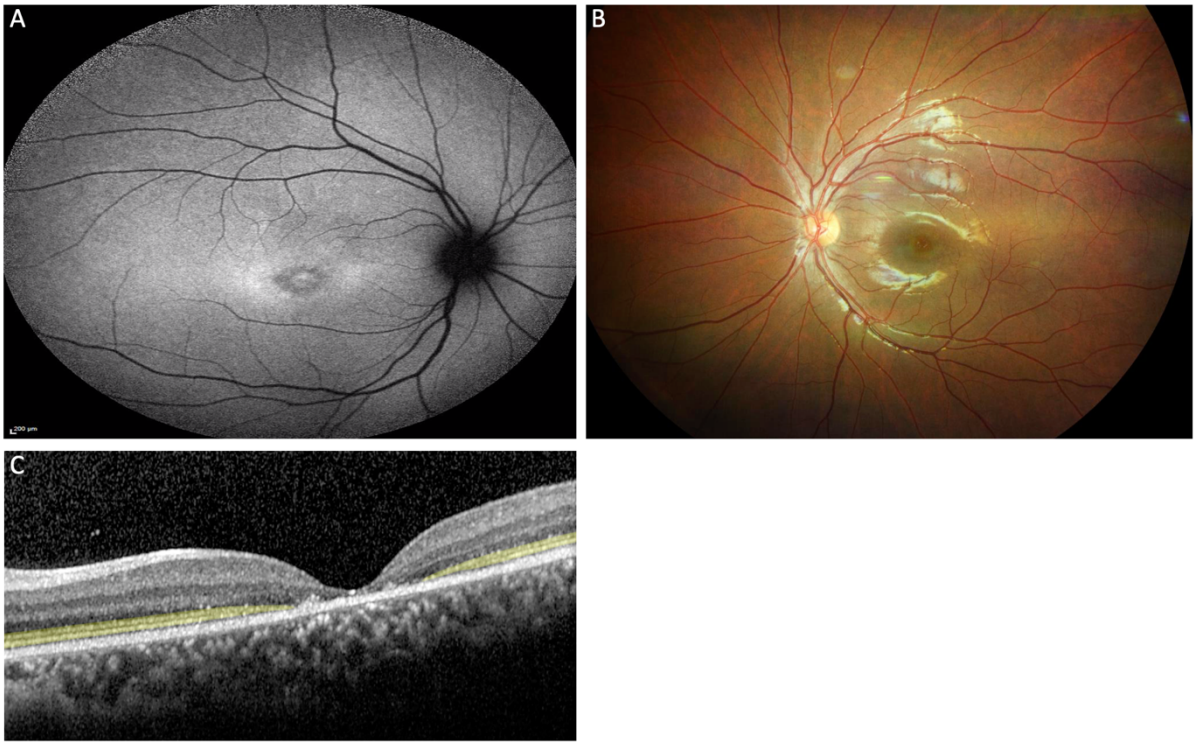

Figure 4.1: Photographs/optical coherence tomography (OCT) scan of the patient's eye. A: Picture showing circular hyperfluorescence around the atrophic foveal region. **B:** Fundus photography picture showing circular macular changes that resemble bull's eye maculopathy. **C:** OCT scan showing absent photoreceptor layer in the macula (yellow).

4.2 Preparation of *ABCA4* variants

Using site-directed mutagenesis, three variants of *ABCA4* plasmids (c.634C>T, c.5882G>A and a combination of these two) were created, followed by transformation and plasmid purification

(section 3.1-3.3). The process of finding mutated clones after site-directed mutagenesis proved to be tedious because of difficulties related to the large size of the ABCA4 cDNA insert. Consequently, several conditions in the analysis had to be modified and tested before the site-directed mutagenesis was successful. To ensure that the ABCA4 insert was present in the plasmids, restriction mapping was performed. Sanger sequencing was performed to ensure that the plasmids harboured the correct mutations. For restriction mapping, the samples were subjected to enzymes cutting binding sites on either side of the insert, proving that the inserts had been introduced into the plasmid (section 3.5, see supplementary Figure 7.2 for agarose gel results). After Sanger sequencing, the sequences of the mutated plasmids were aligned to the reference sequence (section 3.6). The sequence alignment showed that each sample harboured the correct missense mutations and proved that there had been no unintended changes.

4.3 Mycoplasma testing

A mycoplasma test was performed for both the HEK293ft and HeLa cell cultures (section 3.9). Samples included cell culture supernatant, a positive control provided in the kit and sterile PBS used as a negative control. The strip tests revealed negative results for the samples from the cell cultures and the negative controls, and positive results for the positive controls (data not shown).

4.4 Western blot analysis for relative protein concentration of *ABCA4* variants

To study the expression levels of *ABCA4* variants, HEK293ft cells were transfected with the three variants of *ABCA4*, in addition to plasmids with EV and WT (section 3.10). The transfected cells were lysed using a mild detergent, and the total protein concentration was measured (section 3.11.2). The calculated protein concentration was used for equal protein loading onto the SDS-PAGE gel (section 3.11.3). Expression of WT and mutant forms of ABCA4 were detected using an antibody against Rho1D4 which is expressed as a C-terminal fusion tag of ABCA4 and an antibody against β-actin was used as an internal control (section 3.11.15). For the western blots, three biological replicates with two technical replicates of each sample were performed. In Figure 4.2, a representative western blot is presented. Different volumes of total protein solutions were loaded onto each SDS-PAGE gel due to the adjustments made according to the results of the total protein concentration measurements.

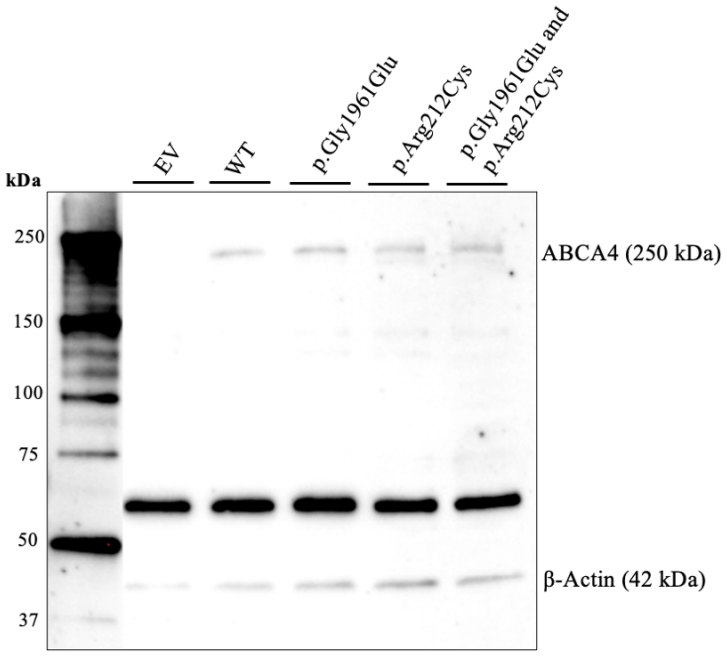

Figure 4.2: Representative western blot of *ABCA4* variants. EV, WT and the *ABCA4* variants were loaded as labelled above the figure. For this membrane, 5.0 µg total protein was loaded onto the SDS-PAGE gel, followed by western blot analysis. The upper bands at 250 kDa correspond to ABCA4 proteins, while the lowest bands at 42 kDa correspond to β-actin. The strong bands in the middle at around 60 kDa are unspecific.

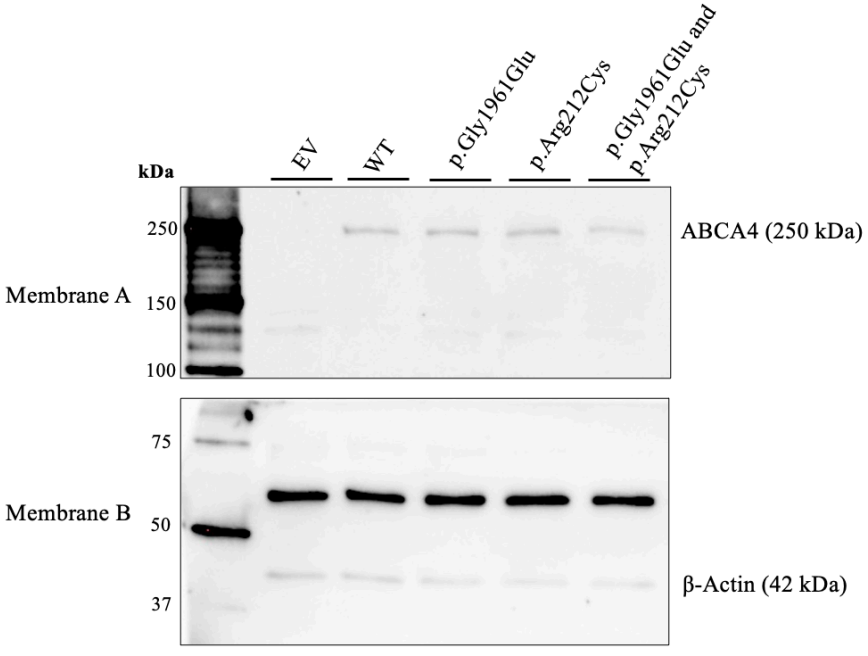

Figure 4.3: Western blot performed to check the unspecific band at 60 kDa. This membrane was handled in the same way as the blot that is presented in Figure 4.2. However, here the membrane was cut in half at around 100 kDa prior to antibody incubation. The top half of the membrane (denoted as membrane A) was incubated with anti-Rho1D4, while the lower half (denoted as membrane B) was incubated with anti-β-actin. The upper bands at 250 kDa correspond to ABCA4 proteins targeted by anti-Rho1D4, while the lowest bands at 42 kDa correspond to β-actin. The strong bands in the middle at around 60 kDa are unspecific.

Figure 4.2 shows bands at the expected molecular weight that correlate to ABCA4 for all samples except for EV. Bands correlating to the molecular weight of β-actin are present in all samples. An unspecific band at around 60 kDa was also present in all samples. This band was seen consistently for all samples that were studied. To ensure that the unspecific band does not appear due to unspecific binding of anti-Rho1D4, the membrane was cut in half at around 100 kDa ahead of antibody incubation. The top half of the membrane (membrane A) was incubated with anti-Rho1D4, while the lower half (membrane B) was incubated with anti-β-actin. The two halves of this membrane are presented in Figure 4.3. The unspecific band still appears on the lower half of the membrane (membrane B).

Using the results of the western blots, the relative protein amount of each band was quantified using the Bio-Rad Image Lab software (section 3.11.15). The intensities of the bands were normalised against the total protein lysate to correct for possible differences in loading quantities. The normalised values were used to determine the relative expression of each variant by setting the expression of WT to 100% and determining the variants' expression as a percentage of this. The average relative expression was calculated for each of the three biological replicates. Using the results from each biological replicate, the average relative expression and the standard deviation of each variant were determined and are presented in Figure 4.4.

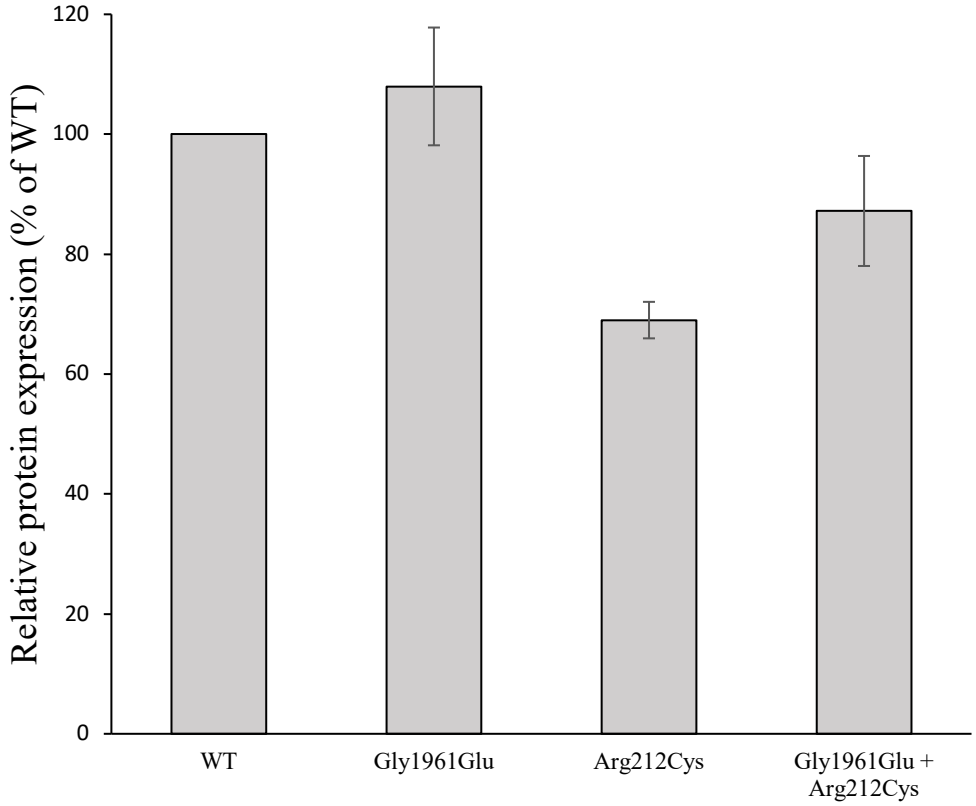

Figure 4.4: Relative protein expression of each variant in % of WT. The height of each bar represents the mean relative expression level for each variant. WT expression is set to 100%. Error bars show the standard deviation between the three biological replicates.

As seen in Figure 4.4, the mean relative expression of p.(Gly1961Glu) is slightly higher but fairly similar to the expression of the WT protein. The mean relative expression of p.(Arg212Cys) is lower than WT, with an expression level of 69%. The double mutation however, showed an intermediate expression level of 87%. The standard deviation between replicates of p.Arg212Cys is rather low, but slightly higher for p.Gly1961Glu and the double mutated protein.

The statistical significance of the normalised protein expression of each variant compared to WT was examined using a two-tailed Student's t-test, assuming unequal variances, where a p-value < 0.05 was considered significant. None of the variants had protein expression levels significantly different from WT.

4.5 RNA quantification through qPCR

The mRNA expression of each variant was analysed using a qPCR TaqMan assay (section 3.16). After RNA purification, the quality and integrity of the samples were checked using an

RNA Screentape assay. For all samples in this study, the RIN-value was higher than 9.8, proving high integrity of all samples (section 3.16.1). cDNA was synthesized from all samples and used in the qPCR TaqMan assay (section 3.16.2). The RNA-quantification was carried out in three biological replicates with two technical replicates. For the qPCR assay, triplicates of each sample were prepared. For this analysis, ACTB and B2M were used as reference housekeeping genes to normalise ABCA4 gene expression (section 3.16.3). The average fold gene expression was normalised against either B2M or ACTB and the standard deviations between biological replicates were calculated for each sample. The results of the normalisation, using ACTB as the reference gene are presented in Figure 4.5. Though not presented in the figure, samples containing cDNA from cells transfected with EV were also included in the analysis. There was no detection of ABCA4, confirming that there is no endogenous expression of ABCA4 in the HEK293f cells used for transfection.

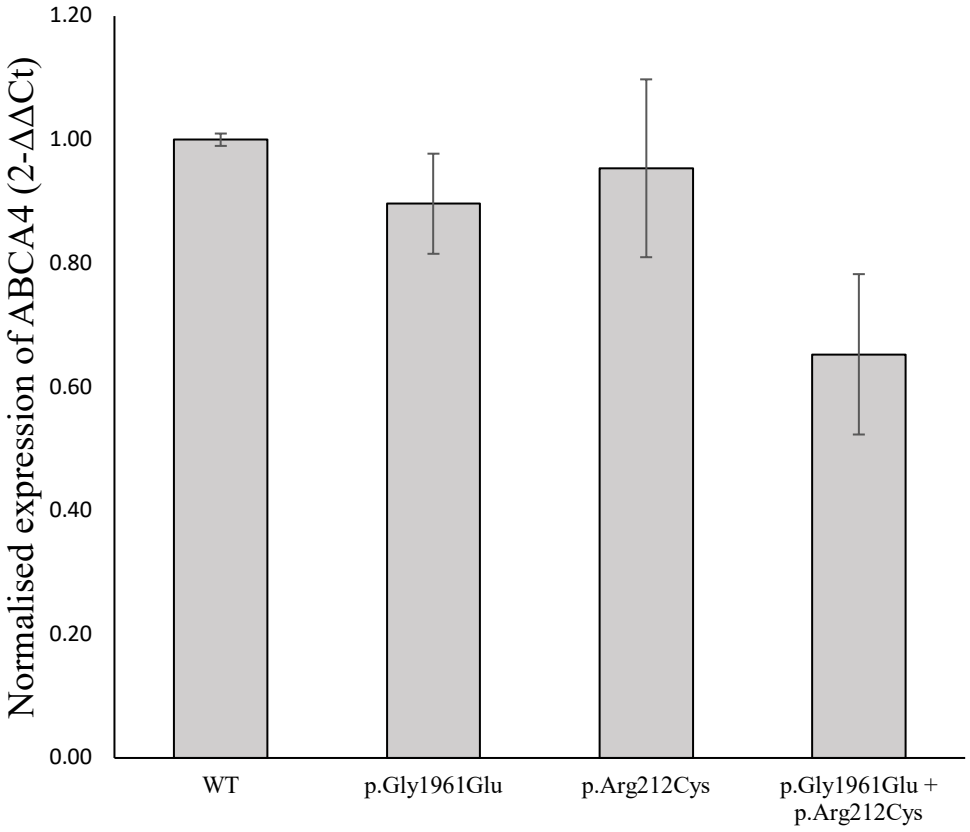

Figure 4.5: Normalised fold gene expression of mRNA in WT and *ABCA4* variants, normalised towards ACTB. Each bar correlates with the denoted variant and shows the mean relative expression of ABCA4 mRNA from three biological replicates. WT has a normalised gene fold expression of 1.00, the p.Gly1961Glu and p.Arg212Cys variants have a value of 0.90-0.95 and the doubly mutated variant has an expression level of 0.65. Error bars show the standard deviation between the three biological replicates.

As seen in Figure 4.5, the levels of expression for all variants are quite similar. The mRNA-expression of WT is 1.00, and both the single mutations also display expression levels close to or around 1.00. When compared to the WT, p.Gly1961Glu and p.Arg212Cys, the double mutated variant with both p.Gly1961Glu and p.Arg212Cys, appears notably lower with a value of 0.65. The statistical significance of each variant's relative gene expression compared to WT was examined by a two-tailed Student's t-test assuming unequal variances, where a p-value < 0.05 was considered significant. For this analysis, none of the variants had significantly different mRNA-expression levels compared to WT ABCA4.

4.6 Localisation of *ABCA4* variants

To investigate the subcellular localisation of the *ABCA4* variants, immunofluorescence was performed on transiently transfected HeLa cells (section 3.18). Overexpressed ABCA4 WT is expected to localise in vesicular-like structures (Garces et al., 2018; Garces et al., 2020). Additionally, the protein tends to co-localise with ER. For variants with a low protein expression, the protein tends to primarily exhibit reticular ER staining (Garces et al., 2018). The HeLa cells were transfected with all variants studied in this thesis, and immunostaining was carried out using anti-Rho1D4 targeting the 1D4-tag of the ABCA4 protein, and anti-calnexin targeting the chaperone protein calnexin in ER. Representative confocal pictures of cells transfected with EV, WT and the variants after immunofluorescence staining are shown in Figure 4.6.

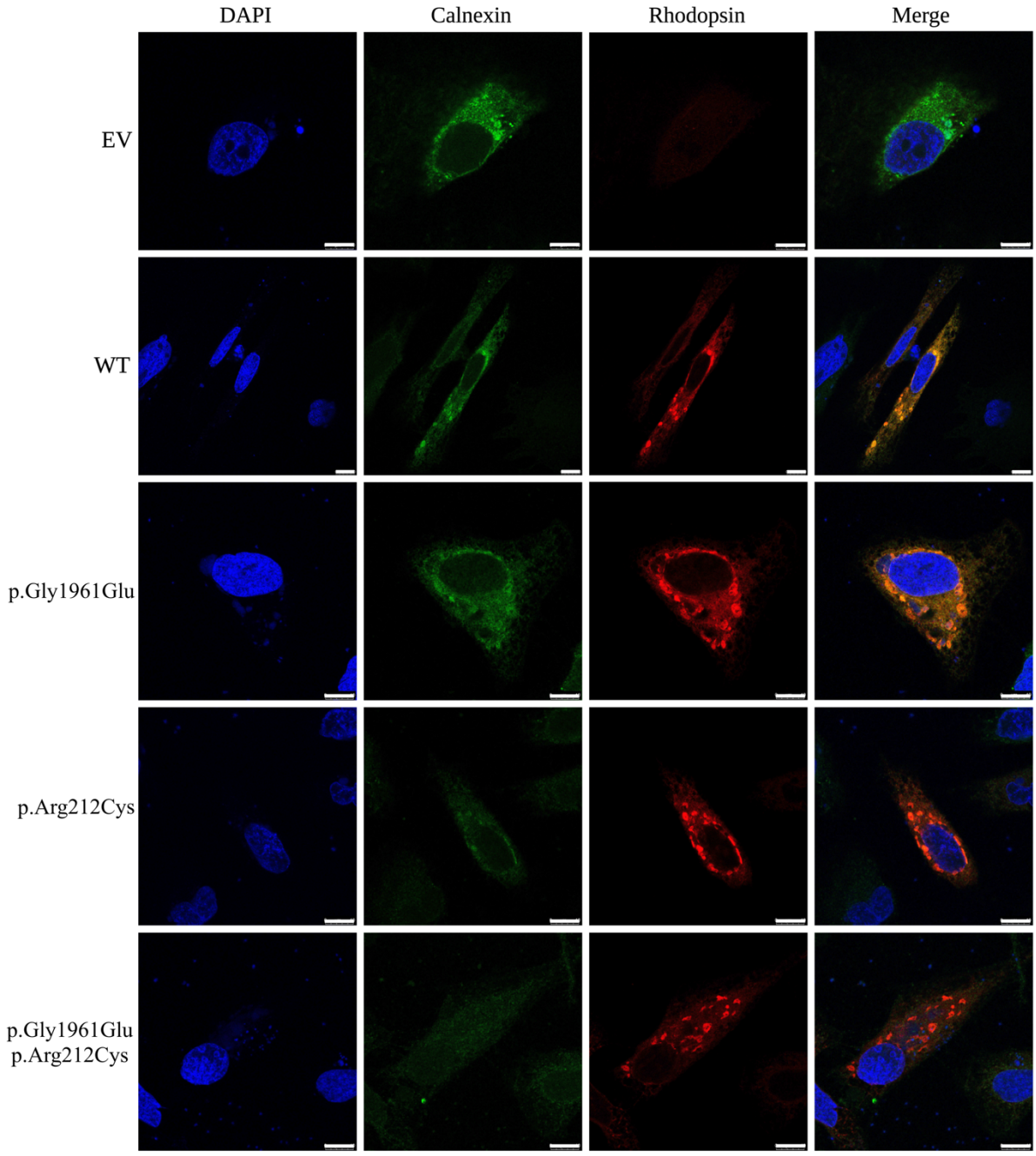

Figure 4.6: Intracellular localisation of ABCA4 in transfected HeLa cells investigated through immunofluorescence. ABCA4 has been targeted with primary antibody mouse anti-Rho1D4 followed by secondary antibody staining using anti-mouse Alexa Fluor 594 (Red). ER was targeted with rabbit anti-calnexin, followed by secondary antibody anti-rabbit Alexa Fluor 488 (Green). The figure shows EV in the first row, WT ABCA4 in the second row, p.Gly1961Glu in the third row, p.Arg212Cys in the fourth row and the double mutated variant containing both p.Gly1961Glu and p.Arg212Cys in the last row. The nuclear DNA in the cells was stained using DAPI (Blue). The pictures were taken using a Leica SP8-STED confocal microscope. The scale bar in the bottom right corner of each picture is 10µm.

As seen in Figure 4.6, the characteristic vesicular structures containing ABCA4 and co-localization with calnexin can be seen for all *ABCA4* variants. As expected, EV shows a negative result for staining with anti-Rho1D4. The co-localization of calnexin and ABCA4 is

particularly seen in the merged pictures of WT and p.Gly1961Glu, displaying an orange-yellow colour. The co-localization can also be seen for p.Arg212Cys and the variant consisting of both p.Gly1961Glu and p.Arg212Cys. For these variants however, the calnexin staining appeared slightly weaker, thus not displaying as strong an orange-yellow colour. The co-localization of calnexin and ABCA4 in vesicular-like structures was also observed in numerous cells not pictured here. This means that the localisation to vesicular-like structures, as is the case for the WT, is present for all variants. Additionally, several cells did not show the localisation of ABCA4 in vesicular-like structures, regardless of being transfected with ABCA4 WT or variants. Representative pictures of these cells are presented in Figure 4.7.

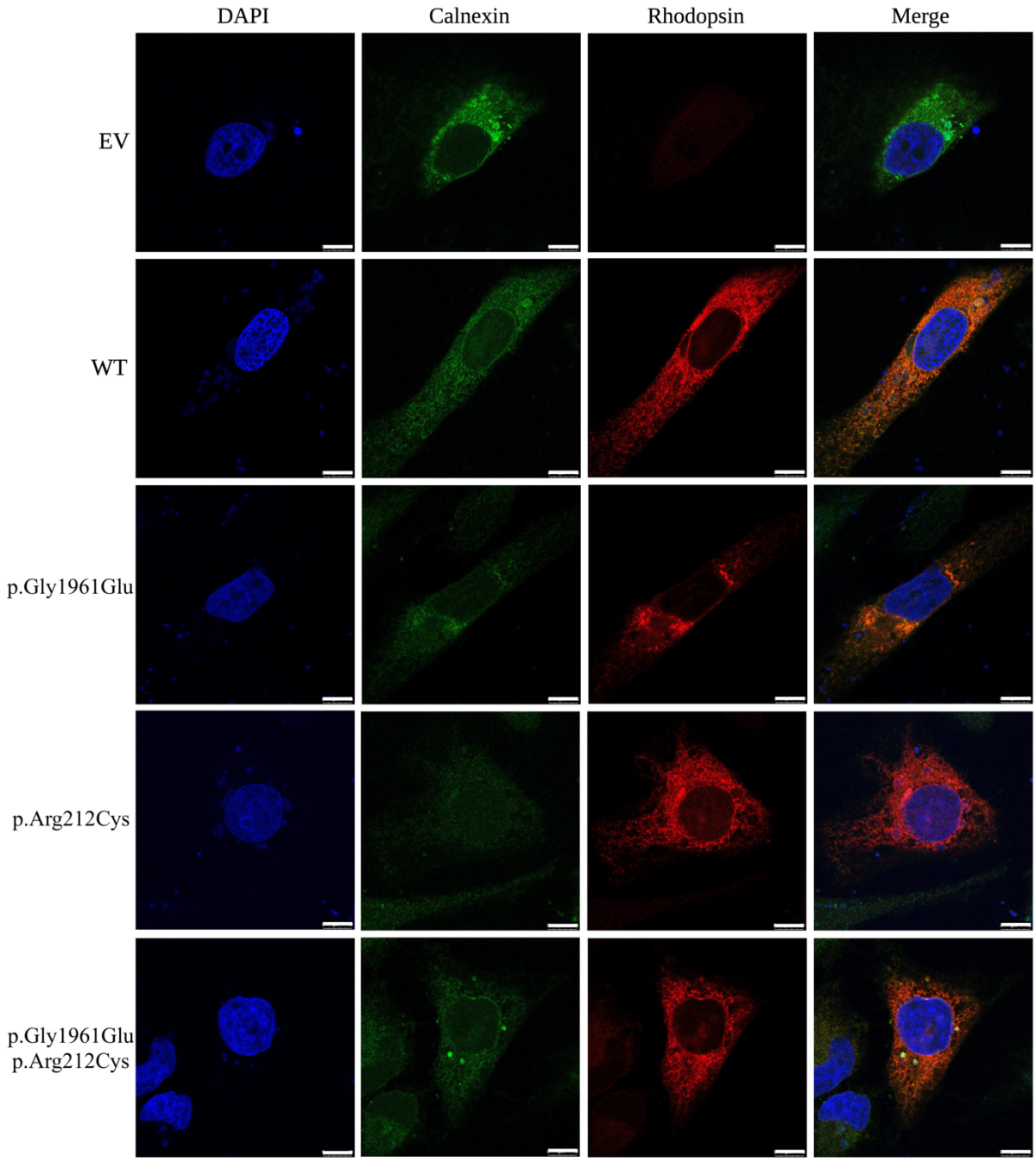

Figure 4.7: Alternative intracellular localisation of ABCA4 in transfected HeLa cells investigated through immunofluorescence. ABCA4 has been targeted with primary antibody mouse anti-Rho1D4 followed by secondary antibody staining using anti-mouse Alexa Fluor 594 (Red). ER was targeted with rabbit anti-calnexin, followed by secondary antibody anti-rabbit Alexa Fluor 488 (Green). The figure shows EV in the first row, WT ABCA4 in the second row, p.Gly1961Glu in the third row, p.Arg212Cys in the fourth row and the double mutated variant containing both p.Gly1961Glu and p.Arg212Cys in the last row. The nuclear DNA in the cells was stained using DAPI (Blue). The pictures were taken using a Leica SP8-STED confocal microscope. The scale bar in the bottom right corner of each picture is 10µm.

4.7 Molecular modelling

The theoretical effect of the variants at the molecular level was investigated using the Alphafold2 modelled ABCA4 protein structure in PyMol (section 3.19). The molecular modelling is shown in Figure 4.8, displaying the protein as a whole, as well as the configuration of the WT protein in the areas where the mutations occur, compared to the mutated variants p.(Gly1961Glu) and p.(Arg212Cys).

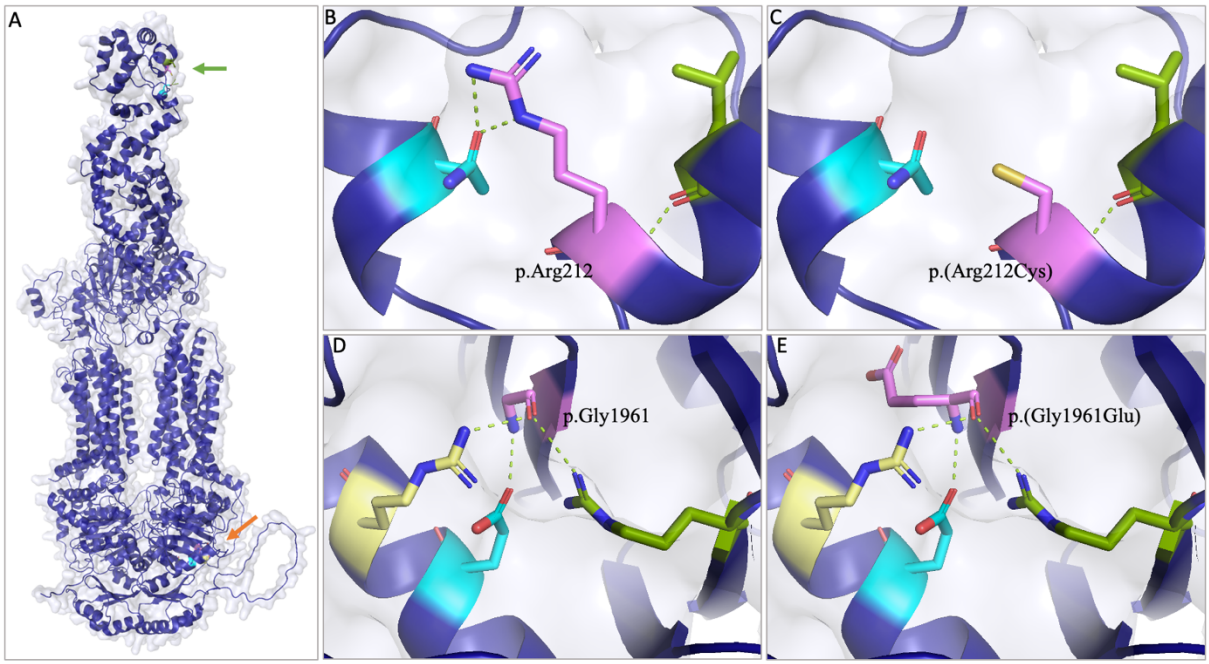

Figure 4.8: Molecular modelling of the *ABCA4* variants. A: A schematic depiction of the ABCA4 protein containing modelled versions of the *ABCA4* variants. Here, the p.(Gly1961Glu) mutation is seen near the bottom of the protein marked with an orange arrow, while the p.(Arg212Cys) mutation is seen towards the top, marked with a green arrow. **B:** Predicted structure of ABCA4 at the position of p.Arg212. Stick figure structures show arginine in this position in pink, as well as all polar contacts that the amino acid makes at this position. The points of contact are displayed with yellow dashes. **C:** Theoretical molecular consequence of the p.(Arg212Cys) mutation. The change in amino acid causes a loss of the polar contact between the amino acid in position 212, and the glutamine depicted in blue. The remaining points of contact are displayed with yellow dashes. **D:** Predicted structure of ABCA4 at the position of p.Gly1961. Stick figure structures show glycine in this position in pink, as well as all polar contacts that this amino acid makes at this position. The points of contact are displayed with yellow dashes. **E:** Theoretical molecular consequence of the p.(Gly1961Glu) mutation. This theoretical model is strained in the position that is displayed here. None of the polar contacts are affected by this mutation and are therefore still displayed with yellow dots.

Displayed in Figure 4.8 are the changes in amino acids that have occurred for the variants studied in this thesis. Figure 4.8A shows that the mutations occur on opposite sides of the protein. Figure 4.8D shows that the glycine in position 1961 partakes in polar contacts with three other amino acids via its peptide backbone, two arginines (Arg1927 in yellow and Arg2139 in green) and a glutamic acid (Glu1924 in blue). The *in silico* site-directed mutagenesis in position 1961 shown in Figure 4.8E indicates that the molecular consequence

of p.(Gly1961Glu) does not affect these polar contacts. However, the substitution may affect the local protein structure through steric clashes. Glutamic acid is considerably larger than glycine and therefore takes up more space in the 1961 position. There are several theoretical steric positioning opportunities for glutamic acid that are likely to affect the protein in different ways. In Figure 4.8B, the WT structure in position 212 is displayed and is seen to create polar contacts to two other amino acids, a leucine (Leu209) via its peptide backbone and a glutamine (Gln190) via the side chain of arginine. When p.(Arg212Cys) occurs (Figure 4.8E), the polar contact to Gln190 is lost.

5. Discussion

Associating the clinical phenotype to genotype in ABCA4-associated retinal dystrophies is difficult, due to the vast spectrum of variants reported and the various combinations of these variants found in individual patients. A large number of pathogenic *ABCA4* variants have therefore been functionally characterised to provide detailed mechanistic information about each mutation. Such detailed knowledge is required to pursue novel therapeutic treatment options. Most patients with ABCA4-related retinal dystrophies are compound heterozygous for two pathogenic variants, but some are homozygous for one single pathogenic variant (Cornelis et al., 2017). The latter group of patients may prove valuable in assessing genotype-phenotype associations, since their clinical presentation may be attributed to a single variant. In the case of the patient that was diagnosed with severe ABCA4-retinopathy at Haukeland University Hospital, which formed the basis of this thesis, *two* pathogenic homozygous variants of *ABCA4* were found: **1)** c.5882G>A, p.(Gly1961Glu), which is associated with mild phenotypes and a later age of onset (Fishman et al., 1999) and **2)** c.634C>T p.(Arg212Cys), which has been associated with more severe phenotypes (Curtis et al., 2020). The patient experienced a severe phenotype that included rapidly reduced visual acuity from the age of 11, red-green colour deficit from the age of 13 and bilateral macular atrophy. The rapid disease progression indicated a synergistic, or at least an additive effect of the two pathogenic variants. After scrutiny of the scientific literature, we noticed that the same combination of two homozygous variants has been reported once previously, in an 11-year-old girl with Stargardt disease (Stone et al., 2017). However, as this girl was reported as part of a large clinical case study, no experimental investigations were performed. In order to understand the molecular mechanisms leading to the severe phenotype, functional studies of these variants, both alone and combined, were carried out.

Functional characterisation was performed using several methods, including analysis of the levels of protein and mRNA expression and subcellular localisation of each variant. The variants p.(Gly1961Glu) and p.(Arg212Cys) were characterised both individually and as a double mutant protein. When characterised together, the variant is here referred to as the double variant. The results from functional characterisations of the variants were all compared to the characteristics of the WT. Plasmids encoding p.(Gly1961Glu), p.(Arg212Cys) and the double variant were created using site-directed mutagenesis and further used to transfect and transiently express the protein in HeLa or HEK293ft cells. As discussed below, the functional

characterisation of the double variant indicated normal stability at the protein level. This is contradictory to the severe phenotype that has been observed in the patient and suggests that the molecular defect of the double mutant may involve ATPase activity or other unknown mechanisms.

5.1 Functional and molecular characterisation

Determining the protein expression level is an important factor in the functional characterisation of *ABCA4* variants, as reduced expression levels are likely to reflect misfolding, decreased stability and loss of function of the protein. Protein expression quantification was carried out using western blot analysis, using samples from transiently transfected HEK293ft cells that had been solubilized. After immunostaining of the membranes, an unspecific band at around 60 kDa was consistently present in every sample as seen in Figures 4.2 and 4.3. As explained in section 4.4, the membrane was cut in half before binding of antibodies, to ensure that this band did not appear due to unspecific binding of anti-Rho1D4. In Figure 4.3, it is clear that the unspecific band is still strongly present in membrane B, which had not been exposed to anti-Rho1D4. Therefore, it is safe to assume that the unspecific band did not appear due to anti-Rho1D4 binding but is rather likely caused by a cross-reaction by the anti-β-actin antibody. From these experiments, it is not possible to identify the origin of this cross-reactive protein. Importantly, this means that the band does not interfere with the results of ABCA4 quantification. Another important point is that the band was present at similar amounts in all samples, including the cells transfected with empty vector, meaning that this band appears regardless of whether the transfected plasmid encodes ABCA4 or not.

As described in section 4.4, the relative protein expression of each variant was determined as a percentage of WT expression. As presented in Figure 4.4, the relative expressions of both the p.Gly1961Glu variant with an expression level of 108%, and the double variant with an expression level of 87% were similar to the WT, indicating a close to normal protein expression for both of these variants. The single mutated p.Arg212Cys variant was expressed lower than WT, at a level of 69%. Both of the single variants have previously been functionally characterised regarding relative protein expression. In a study characterising the p.Arg212Cys variant, the relative protein expression was determined to be 54% (Curtis et al., 2020), while the p.Gly1961Glu variant has shown a relative protein expression of 102% (Garces et al., 2018). When taking the standard deviations into account, the reported protein expression of

p.Arg212Cys and p.Gly1961Glu and the results in this thesis are within the same range. In this study, the double variant has an intermediate relative protein expression, when compared to the two single mutated variants. As the p.Arg212Cys variant is present, it would be natural to assume that the effect of this mutation would at least have caused a similarly low protein expression of the double variant. However, as seen in Figure 4.4, when expressed in combination with the p.Gly1961Glu mutation, the expression appears higher than that of the single p.Arg212Cys variant. As the p.Gly1961Glu variant tends to have a higher protein expression than WT ABCA4, a possible reason for the intermediate protein expression of the double variant could be that the low protein expression of the p.Arg212Cys variant is rescued by a high p.Gly1961Glu expression.

As stated above, the reduction of protein expression can be an important reason for ABCA4 loss of function in patients with ABCA4-related retinopathies. In the case of patients that carry a single homozygous variant of p.Arg212Cys, there is a correlation between protein expression and phenotype (Curtis et al., 2020). These patients tend to have a severe phenotype, which correlates well with the low protein expression compared to WT ABCA4, as shown in this thesis as well as other studies. In contrast, such correlation does not exist to the same extent for the patient with the double variant, as this variant displayed an expression level comparable to normal ABCA4, even though the patient presents with a severe phenotype. This has previously been reported for other variants of ABCA4, where protein expression does not correlate with the remaining function of the protein (Molday et al., 2022).

To correct for possible differences in transfection between variants, the mRNA levels of each variant were quantified. The procedure was carried out using RNA from transiently transfected HEK293ft cells. The results from the qPCR were normalised to facilitate comparisons between the expression of WT and the variants. The mean relative expressions of all the variants were similar or close to the expression of WT. This suggests a limited variation in transfection efficiency between variants and also indicates that all variants express normal mRNA expression levels.

The subcellular localisation of the variants of *ABCA4* was studied through immunofluorescence. Studying the subcellular localisation of each variant provides important knowledge about protein localisation. Additionally, the method provides information about the stability of the variants, as misfolded and aggregated proteins are typically retained in the ER

(Garces et al., 2020). As explained in section 3.18, cultured HeLa cells were transiently transfected with each of the variants. The cells were then incubated with primary antibodies targeting the 1D4-tag and calnexin and then stained with immunofluorescent secondary antibodies.

WT ABCA4 tends to localise to intracellular vesicle-like structures and ER, co-localising with calnexin (Garces et al., 2018; Zhang et al., 2009). This is displayed in Figure 4.6. The cells transfected with EV were used as a negative control for the ABCA4 inserts, confirming that the positive signals are coming from the 1D4-tag and is not an expression induced by the vector itself. The vesicular-like expression patterns were found in the cells of all variants that are studied here, which means that the intracellular localisation appears to be normal for the p.Gly1961Glu variant, the p.Arg212Cys variant and for the double variant. A normal expression pattern for the p.Gly1961Glu variant has also been reported in earlier studies (Garces et al., 2018). For the other two variants, immunofluorescence assays to study the subcellular localisation have not been described previously.

For all the variants, there is also a co-localisation with calnexin, both in the vesicles and in the ER. As displayed in Figure 4.7, we also observed many cells where the protein did not localise to vesicles, but instead displayed reticular staining in the ER, still co-localising with calnexin. Nevertheless, this localisation pattern was present for both the WT and the pathogenic variants, meaning that this is a normal localisation characteristic of ABCA4 in cultured HeLa cells. In the cell that is shown for the double variant (Figure 4.7), there are three vesicular-like structures in green present. However, as seen in the figure, the vesicle-like structures have not been targeted by anti-Rho1D4, meaning that for this cell, these structures contain calnexin only and not ABCA4.

The next step in the functional characterisation would be to study the ATPase activity of the *ABCA4* variants. The ATPase activities of several variants have been determined in previous studies (Molday et al., 2022). To study the effect of *ABCA4* variants on the binding, transport and ATP hydrolysis of the protein, several methods have been reported. Initial approaches included that the variants were purified, reconstituted into liposomes, and then tested for both basal and retinal-stimulated ATPase activities (Sun et al., 1999). In later studies, the variants have not been reconstituted into liposomes, but solubilized in detergent, purified and then the basal and retinal-stimulated ATPase activities have been tested (Curtis et al., 2020).

The measurements of the basal and retinal-stimulated ATPase activities are then used to determine the relative ATPase activity for each variant. A method used to compare the ATPase activities and functionality of *ABCA4* variants is to calculate the E-factor, S-factor and then the F-index. The S-factor is calculated by subtracting the basal ATPase activity of the variant from the N-Ret-PE-activated ATPase activity, which is then divided by the WT N-Ret-PE-activated ATPase activity minus WT basal ATPase activity. E-factor is calculated by dividing the variant protein expression by WT protein expression, and the F-index is then calculated from these two factors by multiplying them (Curtis et al., 2020). The F-index of WT ABCA4 is 1.0, an F-index < 0.15 is typically associated with severe phenotypes, and generally, a relatively high F-index > 0.5 is associated with mild phenotypes (Molday et al., 2022).

The p.Arg212Cys variant has an S-factor of 0.02, and an F-index of 0.01 (Curtis et al., 2020). Based on its F-index, the variant has been classified as severe. This correlates with the phenotype of patients that are homozygous carriers of this variant. The p.Gly1961Glu variant has been extensively studied and is associated with phenotypes on the milder end of the disease spectrum (Burke et al., 2012). Surprisingly, previous studies report that the ATPase activity for this variant is close to virtually undetectable above background noise (Garces et al., 2018). However, this is most likely due to its instability in the solubilization buffer containing CHAPS detergent and does not seem to resemble its actual ATPase activity level (Molday et al., 2022). New methods should therefore be developed to determine the true ATPase activity for this variant.

Because of the problems related to the determination of ATPase activity of the p.Gly1961Glu variant, in addition to time limitations, the ATPase activity was not determined as a part of the functional characterisation in this thesis. It can be assumed that the double variant will be unstable and aggregate similarly to the single mutated p.Gly1961Glu variant when solubilized, and the ATPase activity for this variant should therefore also be investigated using a strategy that does not require CHAPS detergent solubilization.

In addition to the functional characterisation carried out *in vitro*, the impact on the protein 3D-structure of the mutations on the ABCA4 protein was investigated through molecular modelling. Several observable and probably impactful changes occur when site-directed mutagenesis is performed *in silico*. As can be seen in Figures 4.8D and 4.8E, the change that

happens at position 1961 probably impacts the structure of the protein. Glutamic acid is notably larger than the glycine that is normally present in the WT protein and is therefore likely to sterically impact the protein in this position. Additionally, glutamic acid holds a negative charge which is going to affect the local environment. If the negative charge is not neutralised, it will cause instability and a likely change in the folding of the protein. As seen in Figure 4.8A, denoted by an orange arrow, this change occurs in the NBD2 part of the protein, meaning that it may affect the ATP binding and NBD dimerization that is important to start the transportation process of N-Ret-PE (Molday et al., 2022). Based on the results of protein expression and subcellular localisation of this variant, it can be assumed that the protein will localise to the membrane with the same or a similar expression as WT. As has been discussed above, the likely cause of loss of function for the p.(Gly1961Glu) variant may be a lower ATPase activity. As the NBDs play an important role in binding ATP, the change happening in position 1961 is likely to affect the whole domain, leading to an altered ATPase activity.

In Figures 4.8B and C, the change that occurs at position 212 is displayed. In WT ABCA4, arginine 212 interacts with leucine 209 via its peptide backbone and glutamine 190 via its side chain. When p.(Arg212Cys) occurs, the polar contact to glutamine 190 is lost. This type of change in amino acids is likely to affect the stability of the protein, which in turn may have an effect on the protein's ability to efficiently participate in substrate transportation. As displayed in Figure 4.8A, the two variants in the double homozygous variant investigated in this study occur on opposite sides of the transmembrane domain of the protein, the p.(Arg212Cys) occurring in ECD1, while the p.(Gly1961Glu) occurs in the NBD2. Therefore, the possible impact that the variants could have had on each other is unlikely to cause an added change in the structure of the protein, as the changes occur in different domains that are spatially distant from one another. However, the reported ATPase activity of p.(Arg212Cys) is low, and even though the ATPase activity of the p.(Gly1961Glu) variant has not properly been determined, it can be presumed that the ATPase activity is likely somewhat affected. As explained, the NBD dimerization through ATP binding is an important process to transport N-Ret-PE, while the ECDs play a part in guiding the substrate into the hydrophobic cavity in the TMD. A possible explanation for the severe phenotype in the patient with the double variant may therefore be that the transport mechanism of the protein is affected both in the ECD1 and the NBD2 domains, leading to a synergistic effect where the overall functionality of the protein is greatly reduced.

5.2 Limitations of methods used for functional characterisation

All the methods used to characterise functionality of the studied *ABCA4* variants were carried out through transient expression in cultured cells. This approach may not fully recapitulate native conditions when ABCA4 proteins are expressed in photoreceptor cells in the eye, including factors such as chaperone proteins that facilitate the folding of proteins (Molday et al., 2022). Therefore, results from the western blot analysis protein expression may in some cases not correlate to the protein expression that occurs for the variant *in vivo.*

For the characterisation of protein expression, western blot analysis was used in a quantitative way, where each band was normalised against the total amount of protein in each sample. In this thesis, β-actin was also intended to be used for normalisation. Due to time limitations, the β-actin normalisation results could not be included as there were problems related to imaging of the membranes. With more time, the western blots would have been repeated to also include normalisation results from β-actin. These issues illustrate a limitation of quantitative western blot analysis. To accurately quantify bands in each membrane, every step in the western blot process must be performed appropriately. While the effect of human error should be accounted for through the use of biological and technical replicates, it is apparent that when using western blots in a quantitative manner, standard deviations are fairly high for each variant. Still, the western blot analysis gives a good indication when it comes to protein expression levels and has traditionally been the preferred method to study protein levels of *ABCA4* variants (Garces et al., 2018; Garces et al., 2020). In order to verify that our western blot analysis is able to detect variants with significantly decreased protein expression, we could also have included previously characterised variants with low expression levels, such as the p.(Leu661Arg) variant (Garces et al., 2020). However, due to time limitations and difficulties in carrying out mutagenesis (see section 4.2), we were not able to include these controls.

There are also limitations related to the method used to determine the subcellular localisation of *ABCA4* variants. Based on results from previous studies, it has been proven that WT ABCA4 will typically localise in vesicular-like structures in the ER and co-localise with calnexin when overexpressed in cultured cells (Garces et al., 2018). The method used to determine subcellular localisation is purely qualitative and includes a somewhat subjective assessment of whether a variant has localised in vesicles and the ER or solely in the ER. The results in this thesis showed that numerous cells did not display vesicular-like structures at all for both the WT and the variants. The method of determining variants that display localisation in both vesicles and ER

as normal, and variants where vesicles cannot be found as likely pathogenic, therefore heavily relies on a successful transient transfection and meticulous exploration of the microscopy slide. Again, in order to verify that the immunofluorescence method is able to detect ABCA4 variants not displaying vesicular localisation, specific variants with such defects could have been included, like p.(Leu661Arg) (Garces et al., 2020).

5.3 Further perspectives

Currently, there are no available treatment options for patients suffering from ABCA4-related retinopathies. Furthermore, attempts to develop gene therapy that works for all variants have been unsuccessful thus far. Consequently, personalised medicine is expected to be the most viable approach for treating these patients. The development of such options is dependent on thorough functional characterisation in order to ascertain the specific disease mechanisms associated with each specific variant so that these mechanisms can be targeted.

The results of the functional characterisation of the double variant performed in this thesis indicate a normal functioning protein. However, based on the phenotype of the patient, it is obvious that this is not the reality. The methods used in this thesis are only part of a complete functional characterisation and are insufficient in explaining the severe phenotype of the patient. Still, the experiments conducted have been important in ruling out protein expression and localisation as the cause of ABCA4 protein dysfunction of the double variant. Further functional characterisation is necessary to completely characterise the double variant, where the first step would be to test the ATPase activity of the double variant using a method where the mutant protein is solubilized and purified. As the likely result of this assay will be similar to the previously reported results of the single mutated p.(Gly1961Glu) variant, the next step would be the development of a method to investigate the ATPase activity without having to solubilize the protein.

Another interesting perspective would be to study the mRNA expression of the variant in cells from the patient, as there is a possibility that the RNA splicing pattern of the double variant could be affected. However, as the mRNA expression level of ABCA4 is low in peripheral blood cells, the analysis would have to be performed using skin fibroblasts or other more inaccessible tissues.

5.4 Concluding remarks

In this study, the aim was to functionally characterise the *ABCA4* variants p.(Gly1961Glu), p.(Arg212Cys) as single variants and a double mutation, as compared to WT ABCA4. A patient under clinical investigation at Haukeland University Hospital was diagnosed with a severe ABCA4-retinopathy caused by homozygosity for a doubly mutated allele consisting of both of the two variants.

The functional characterisation of the variants included analysis of the relative protein expression quantified through western blotting, mRNA expression and intracellular localisation which was analysed using immunofluorescence. In total, the functional characterisation of the double variant showed that the protein expression, mRNA expression and subcellular localisation were similar to the WT ABCA4. Molecular modelling indicated a potential of the two investigated mutations to disrupt critical amino acid interactions and protein stability and is likely a cause of reduced ATPase activity. The severe phenotype associated with the double mutation may be attributed to a synergistic effect of the mutations occurring in distinct protein domains that have different roles in substrate transport.

The partial functional characterisation revealed a discrepancy between the double variant and the severe phenotype in the patient, which means that the methods used to characterise the variant here are insufficient in explaining the cause of the phenotype. Therefore, to further investigate the double variant, a new ATPase activity assay to study the double variant should be developed, and the mRNA expression in the patient's fibroblasts should be studied.

6. References

Al-Khuzaei, S., Broadgate, S., Foster, C. R., Shah, M., Yu, J., Downes, S. M., & Halford, S. (2021). An Overview of the Genetics of ABCA4 Retinopathies, an Evolving Story. *Genes (Basel)*, *12*(8). https://doi.org/10.3390/genes12081241

Allikmets, R., Shroyer, N. F., Singh, N., Seddon, J. M., Lewis, R. A., Bernstein, P. S., Peiffer, A., Zabriskie, N. A., Li, Y., Hutchinson, A., Dean, M., Lupski, J. R., & Leppert, M. (1997). Mutation of the Stargardt disease gene (ABCR) in age-related macular degeneration. *Science*, *277*(5333), 1805-1807. https://doi.org/10.1126/science.277.5333.1805

Anderson, R. E., & Maude, M. B. (1970). Lipids of ocular tissues. 6. Phospholipids of bovine rod outer segments. *Biochemistry*, *9*(18), 3624-3628. https://doi.org/10.1021/bi00820a019

Azarian, S. M., & Travis, G. H. (1997). The photoreceptor rim protein is an ABC transporter encoded by the gene for recessive Stargardt's disease (ABCR). *FEBS Lett*, *409*(2), 247-252. https://doi.org/10.1016/s0014-5793(97)00517-6

Bauwens, M., Garanto, A., Sangermano, R., Naessens, S., Weisschuh, N., De Zaeytijd, J., Khan, M., Sadler, F., Balikova, I., Van Cauwenbergh, C., Rosseel, T., Bauwens, J., De Leeneer, K., De Jaegere, S., Van Laethem, T., De Vries, M., Carss, K., Arno, G., Fakin, A., . . . De Baere, E. (2019). ABCA4-associated disease as a model for missing heritability in autosomal recessive disorders: novel noncoding splice, cis-regulatory, structural, and recurrent hypomorphic variants. *Genet Med*, *21*(8), 1761-1771. https://doi.org/10.1038/s41436-018-0420-y

Beharry, S., Zhong, M., & Molday, R. S. (2004). N-retinylidene-phosphatidylethanolamine is the preferred retinoid substrate for the photoreceptor-specific ABC transporter ABCA4 (ABCR). *J Biol Chem*, *279*(52), 53972-53979. https://doi.org/10.1074/jbc.M405216200

Ben-Shabat, S., Parish, C. A., Vollmer, H. R., Itagaki, Y., Fishkin, N., Nakanishi, K., & Sparrow, J. R. (2002). Biosynthetic studies of A2E, a major fluorophore of retinal pigment epithelial lipofuscin. *J Biol Chem*, *277*(9), 7183-7190. https://doi.org/10.1074/jbc.M108981200

Bertelsen, M., Zernant, J., Larsen, M., Duno, M., Allikmets, R., & Rosenberg, T. (2014). Generalized choriocapillaris dystrophy, a distinct phenotype in the spectrum of ABCA4-associated retinopathies. *Invest Ophthalmol Vis Sci*, *55*(4), 2766-2776. https://doi.org/10.1167/iovs.13-13391

Bungert, S., Molday, L. L., & Molday, R. S. (2001). Membrane topology of the ATP binding cassette transporter ABCR and its relationship to ABC1 and related ABCA transporters: identification of N-linked glycosylation sites. *J Biol Chem*, *276*(26), 23539-23546. https://doi.org/10.1074/jbc.M101902200

Burke, T. R., Duncker, T., Woods, R. L., Greenberg, J. P., Zernant, J., Tsang, S. H., Smith, R. T., Allikmets, R., Sparrow, J. R., & Delori, F. C. (2014). Quantitative fundus autofluorescence in recessive Stargardt disease. *Invest Ophthalmol Vis Sci*, *55*(5), 2841-2852. https://doi.org/10.1167/iovs.13-13624

Burke, T. R., Fishman, G. A., Zernant, J., Schubert, C., Tsang, S. H., Smith, R. T., Ayyagari, R., Koenekoop, R. K., Umfress, A., Ciccarelli, M. L., Baldi, A., Iannaccone, A., Cremers, F. P., Klaver, C. C., & Allikmets, R. (2012). Retinal phenotypes in patients homozygous for the G1961E mutation in the ABCA4 gene. *Invest Ophthalmol Vis Sci*, *53*(8), 4458-4467. https://doi.org/10.1167/iovs.11-9166

Cella, W., Greenstein, V. C., Zernant-Rajang, J., Smith, T. R., Barile, G., Allikmets, R., & Tsang, S. H. (2009). G1961E mutant allele in the Stargardt disease gene ABCA4 causes bull's eye maculopathy. *Exp Eye Res*, *89*(1), 16-24. https://doi.org/10.1016/j.exer.2009.02.001

Chen, S., Francioli, L. C., Goodrich, J. K., Collins, R. L., Kanai, M., Wang, Q., Alföldi, J., Watts, N. A., Vittal, C., Gauthier, L. D., Poterba, T., Wilson, M. W., Tarasova, Y., Phu, W., Yohannes, M. T., Koenig, Z., Farjoun, Y., Banks, E., Donnelly, S., . . . Karczewski, K. J. (2022). A genome-wide mutational constraint map quantified from variation in 76,156 human genomes. *bioRxiv*, 2022.2003.2020.485034. https://doi.org/10.1101/2022.03.20.485034

Cornelis, S. S., Bax, N. M., Zernant, J., Allikmets, R., Fritsche, L. G., den Dunnen, J. T., Ajmal, M., Hoyng, C. B., & Cremers, F. P. (2017). In Silico Functional Meta-Analysis of 5,962 ABCA4 Variants in 3,928 Retinal Dystrophy Cases. *Hum Mutat*, *38*(4), 400-408. https://doi.org/10.1002/humu.23165

Cremers, F. P., van de Pol, D. J., van Driel, M., den Hollander, A. I., van Haren, F. J., Knoers, N. V., Tijmes, N., Bergen, A. A., Rohrschneider, K., Blankenagel, A., Pinckers, A. J., Deutman, A. F., & Hoyng, C. B. (1998). Autosomal recessive retinitis pigmentosa and cone-rod dystrophy caused by splice site mutations in the Stargardt's disease gene ABCR. *Hum Mol Genet*, *7*(3), 355-362. https://doi.org/10.1093/hmg/7.3.355

Cremers, F. P. M., Lee, W., Collin, R. W. J., & Allikmets, R. (2020). Clinical spectrum, genetic complexity and therapeutic approaches for retinal disease caused by ABCA4 mutations. *Prog Retin Eye Res*, *79*, 100861. https://doi.org/10.1016/j.preteyeres.2020.100861

Curtis, S. B., Molday, L. L., Garces, F. A., & Molday, R. S. (2020). Functional analysis and classification of homozygous and hypomorphic ABCA4 variants associated with Stargardt macular degeneration. *Hum Mutat*, *41*(11), 1944-1956. https://doi.org/10.1002/humu.24100

Ding, J. D., Salinas, R. Y., & Arshavsky, V. Y. (2015). Discs of mammalian rod photoreceptors form through the membrane evagination mechanism. *J Cell Biol*, *211*(3), 495-502. https://doi.org/10.1083/jcb.201508093

Ducroq, D., Rozet, J. M., Gerber, S., Perrault, I., Barbet, D., Hanein, S., Hakiki, S., Dufier, J. L., Munnich, A., Hamel, C., & Kaplan, J. (2002). The ABCA4 gene in autosomal recessive cone-rod dystrophies. *Am J Hum Genet*, *71*(6), 1480-1482. https://doi.org/10.1086/344829

Fishman, G. A., Stone, E. M., Grover, S., Derlacki, D. J., Haines, H. L., & Hockey, R. R. (1999). Variation of clinical expression in patients with Stargardt dystrophy and sequence variations in the ABCR gene. *Arch Ophthalmol*, *117*(4), 504-510. https://doi.org/10.1001/archopht.117.4.504

Garces, F., Jiang, K., Molday, L. L., Stöhr, H., Weber, B. H., Lyons, C. J., Maberley, D., & Molday, R. S. (2018). Correlating the Expression and Functional Activity of ABCA4 Disease Variants With the Phenotype of Patients With Stargardt Disease. *Invest Ophthalmol Vis Sci*, *59*(6), 2305-2315. https://doi.org/10.1167/iovs.17-23364

Garces, F. A., Scortecci, J. F., & Molday, R. S. (2020). Functional Characterization of ABCA4 Missense Variants Linked to Stargardt Macular Degeneration. *Int J Mol Sci*, *22*(1). https://doi.org/10.3390/ijms22010185

Gregersen, N. (2006). Protein misfolding disorders: pathogenesis and intervention. *J Inherit Metab Dis*, *29*(2-3), 456-470. https://doi.org/10.1007/s10545-006-0301-4

Hall, J. E. (2011). The Eye: II. Receptor and Neural Function of the Retina. In *Guyton and Hall Textbook of Medical Physiology* (12 ed.). W B Saunders.

Holtan, J. P., Aukrust, I., Jansson, R. W., Berland, S., Bruland, O., Gjerde, B. L., Stokowy, T., Bojovic, O., Forsaa, V., Austeng, D., Rødahl, E., Bredrup, C., Knappskog, P. M., & Bragadóttir, R. (2021). Clinical features and molecular genetics of patients with ABCA4-retinal dystrophies. *Acta Ophthalmol*, *99*(5), e733-e746. https://doi.org/10.1111/aos.14679

Holtan, J. P., Selmer, K. K., Heimdal, K. R., & Bragadóttir, R. (2020). Inherited retinal disease in Norway - a characterization of current clinical and genetic knowledge. *Acta Ophthalmol*, *98*(3), 286-295. https://doi.org/10.1111/aos.14218

Jumper, J., Evans, R., Pritzel, A., Green, T., Figurnov, M., Ronneberger, O., Tunyasuvunakool, K., Bates, R., Žídek, A., Potapenko, A., Bridgland, A., Meyer, C., Kohl, S. A. A., Ballard, A. J., Cowie, A., Romera-Paredes, B., Nikolov, S., Jain, R., Adler, J., . . . Hassabis, D. (2021). Highly accurate protein structure prediction with AlphaFold. *Nature*, *596*(7873), 583-589. https://doi.org/10.1038/s41586-021-03819-2

Klevering, B. J., Blankenagel, A., Maugeri, A., Cremers, F. P., Hoyng, C. B., & Rohrschneider, K. (2002). Phenotypic spectrum of autosomal recessive cone-rod dystrophies caused by mutations in the ABCA4 (ABCR) gene. *Invest Ophthalmol Vis Sci*, *43*(6), 1980-1985.

Klevering, B. J., Deutman, A. F., Maugeri, A., Cremers, F. P., & Hoyng, C. B. (2005). The spectrum of retinal phenotypes caused by mutations in the ABCA4 gene. *Graefes Arch Clin Exp Ophthalmol*, *243*(2), 90-100. https://doi.org/10.1007/s00417-004-1079-4

Lambertus, S., van Huet, R. A., Bax, N. M., Hoefsloot, L. H., Cremers, F. P., Boon, C. J., Klevering, B. J., & Hoyng, C. B. (2015). Early-onset stargardt disease: phenotypic and genotypic characteristics. *Ophthalmology*, *122*(2), 335-344. https://doi.org/10.1016/j.ophtha.2014.08.032

Landrum, M. J., Lee, J. M., Benson, M., Brown, G. R., Chao, C., Chitipiralla, S., Gu, B., Hart, J., Hoffman, D., Jang, W., Karapetyan, K., Katz, K., Liu, C., Maddipatla, Z., Malheiro, A.,

McDaniel, K., Ovetsky, M., Riley, G., Zhou, G., . . . Maglott, D. R. (2018). ClinVar: improving access to variant interpretations and supporting evidence. *Nucleic Acids Res*, *46*(D1), D1062-d1067. https://doi.org/10.1093/nar/gkx1153

Liu, F., Lee, J., & Chen, J. (2021). Molecular structures of the eukaryotic retinal importer ABCA4. *Elife*, *10*. https://doi.org/10.7554/eLife.63524

Liu, J., Itagaki, Y., Ben-Shabat, S., Nakanishi, K., & Sparrow, J. R. (2000). The biosynthesis of A2E, a fluorophore of aging retina, involves the formation of the precursor, A2-PE, in the photoreceptor outer segment membrane. *J Biol Chem*, *275*(38), 29354-29360. https://doi.org/10.1074/jbc.M910191199

MacKenzie, D., Arendt, A., Hargrave, P., McDowell, J. H., & Molday, R. S. (1984). Localization of binding sites for carboxyl terminal specific anti-rhodopsin monoclonal antibodies using synthetic peptides. *Biochemistry*, *23*(26), 6544-6549. https://doi.org/10.1021/bi00321a041

Martínez-Mir, A., Paloma, E., Allikmets, R., Ayuso, C., del Rio, T., Dean, M., Vilageliu, L., Gonzàlez-Duarte, R., & Balcells, S. (1998). Retinitis pigmentosa caused by a homozygous mutation in the Stargardt disease gene ABCR. *Nat Genet*, *18*(1), 11-12. https://doi.org/10.1038/ng0198-11

Maugeri, A., Flothmann, K., Hemmrich, N., Ingvast, S., Jorge, P., Paloma, E., Patel, R., Rozet, J. M., Tammur, J., Testa, F., Balcells, S., Bird, A. C., Brunner, H. G., Hoyng, C. B., Metspalu, A., Simonelli, F., Allikmets, R., Bhattacharya, S. S., D'Urso, M., . . . Cremers, F. P. (2002). The ABCA4 2588G>C Stargardt mutation: single origin and increasing frequency from South-West to North-East Europe. *Eur J Hum Genet*, *10*(3), 197-203. https://doi.org/10.1038/sj.ejhg.5200784

Maugeri, A., Klevering, B. J., Rohrschneider, K., Blankenagel, A., Brunner, H. G., Deutman, A. F., Hoyng, C. B., & Cremers, F. P. (2000). Mutations in the ABCA4 (ABCR) gene are the major cause of autosomal recessive cone-rod dystrophy. *Am J Hum Genet*, *67*(4), 960-966. https://doi.org/10.1086/303079

Michaelides, M., Hunt, D. M., & Moore, A. T. (2003). The genetics of inherited macular dystrophies. *Journal of Medical Genetics*, *40*(9), 641-650. https://doi.org/10.1136/jmg.40.9.641

Molday, R. S., Garces, F. A., Scortecci, J. F., & Molday, L. L. (2022). Structure and function of ABCA4 and its role in the visual cycle and Stargardt macular degeneration. *Prog Retin Eye Res*, *89*, 101036. https://doi.org/10.1016/j.preteyeres.2021.101036

Molday, R. S., & Zhang, K. (2010). Defective lipid transport and biosynthesis in recessive and dominant Stargardt macular degeneration. *Prog Lipid Res*, *49*(4), 476-492. https://doi.org/10.1016/j.plipres.2010.07.002

Papermaster, D. S., Converse, C. A., & Zorn, M. (1976). Biosynthetic and immunochemical characterization of large protein in frog and cattle rod outer segment membranes. *Exp Eye Res*, *23*(2), 105-115. https://doi.org/10.1016/0014-4835(76)90194-9

Poincelot, R. P., Millar, P. G., Kimbel, R. L., Jr., & Abrahamson, E. W. (1969). Lipid to protein chromophore transfer in the photolysis of visual pigments. *Nature*, *221*(5177), 256-257. https://doi.org/10.1038/221256a0

Quazi, F., & Molday, R. S. (2014). ATP-binding cassette transporter ABCA4 and chemical isomerization protect photoreceptor cells from the toxic accumulation of excess 11-cis-retinal. *Proc Natl Acad Sci U S A*, *111*(13), 5024-5029. https://doi.org/10.1073/pnas.1400780111

Rotenstreich, Y., Fishman, G. A., & Anderson, R. J. (2003). Visual acuity loss and clinical observations in a large series of patients with Stargardt disease. *Ophthalmology*, *110*(6), 1151-1158. https://doi.org/10.1016/s0161-6420(03)00333-6

Runhart, E. H., Sangermano, R., Cornelis, S. S., Verheij, J., Plomp, A. S., Boon, C. J. F., Lugtenberg, D., Roosing, S., Bax, N. M., Blokland, E. A. W., Jacobs-Camps, M. H. M., van der Velde-Visser, S. D., Pott, J. R., Rohrschneider, K., Thiadens, A., Klaver, C. C. W., van den Born, L. I., Hoyng, C. B., & Cremers, F. P. M. (2018). The Common ABCA4 Variant p.Asn1868Ile Shows Nonpenetrance and Variable Expression of Stargardt Disease When Present in trans With Severe Variants. *Invest Ophthalmol Vis Sci*, *59*(8), 3220-3231. https://doi.org/10.1167/iovs.18-23881

Sakai, N., Decatur, J., & Nakanishi, K. (1996). Ocular Age Pigment “A2-E”: An Unprecedented Pyridinium Bisretinoid. *American Chemical Society*.

Sparrow, J. R., & Boulton, M. (2005). RPE lipofuscin and its role in retinal pathobiology. *Exp Eye Res*, *80*(5), 595-606. https://doi.org/10.1016/j.exer.2005.01.007
Sparrow, J. R., Kim, S. R., Cuervo, A. M., & Bandhyopadhyayand, U. (2008). A2E, a pigment of RPE lipofuscin, is generated from the precursor, A2PE by a lysosomal enzyme activity. *Adv Exp Med Biol*, *613*, 393-398. https://doi.org/10.1007/978-0-387-74904-4_46
Stone, E. M., Andorf, J. L., Whitmore, S. S., DeLuca, A. P., Giacalone, J. C., Streb, L. M., Braun, T. A., Mullins, R. F., Scheetz, T. E., Sheffield, V. C., & Tucker, B. A. (2017). Clinically Focused Molecular Investigation of 1000 Consecutive Families with Inherited Retinal Disease. *Ophthalmology*, *124*(9), 1314-1331. https://doi.org/10.1016/j.ophtha.2017.04.008
Strauss, O. (2005). The retinal pigment epithelium in visual function. *Physiol Rev*, *85*(3), 845-881. https://doi.org/10.1152/physrev.00021.2004
Strauss, R. W., Ho, A., Muñoz, B., Cideciyan, A. V., Sahel, J. A., Sunness, J. S., Birch, D. G., Bernstein, P. S., Michaelides, M., Traboulsi, E. I., Zrenner, E., Sadda, S., Ervin, A. M., West, S., & Scholl, H. P. (2016). The Natural History of the Progression of Atrophy Secondary to Stargardt Disease (ProgStar) Studies: Design and Baseline Characteristics: ProgStar Report No. 1. *Ophthalmology*, *123*(4), 817-828. https://doi.org/10.1016/j.ophtha.2015.12.009
Sun, H., Molday, R. S., & Nathans, J. (1999). Retinal stimulates ATP hydrolysis by purified and reconstituted ABCR, the photoreceptor-specific ATP-binding cassette transporter responsible for Stargardt disease. *J Biol Chem*, *274*(12), 8269-8281. https://doi.org/10.1074/jbc.274.12.8269
Saari, J. C. (2000). Biochemistry of visual pigment regeneration: the Friedenwald lecture. *Invest Ophthalmol Vis Sci*, *41*(2), 337-348.
Saari, J. C. (2012). Vitamin A metabolism in rod and cone visual cycles. *Annu Rev Nutr*, *32*, 125-145. https://doi.org/10.1146/annurev-nutr-071811-150748
Tanna, P., Strauss, R. W., Fujinami, K., & Michaelides, M. (2017). Stargardt disease: clinical features, molecular genetics, animal models and therapeutic options. *Br J Ophthalmol*, *101*(1), 25-30. https://doi.org/10.1136/bjophthalmol-2016-308823
Tsybovsky, Y., Molday, R. S., & Palczewski, K. (2010). The ATP-binding cassette transporter ABCA4: structural and functional properties and role in retinal disease. *Adv Exp Med Biol*, *703*, 105-125. https://doi.org/10.1007/978-1-4419-5635-4_8
Varadi, M., Anyango, S., Deshpande, M., Nair, S., Natassia, C., Yordanova, G., Yuan, D., Stroe, O., Wood, G., Laydon, A., Žídek, A., Green, T., Tunyasuvunakool, K., Petersen, S., Jumper, J., Clancy, E., Green, R., Vora, A., Lutfi, M., . . . Velankar, S. (2022). AlphaFold Protein Structure Database: massively expanding the structural coverage of protein-sequence space with high-accuracy models. *Nucleic Acids Res*, *50*(D1), D439-d444. https://doi.org/10.1093/nar/gkab1061
Wang, J. S., & Kefalov, V. J. (2011). The cone-specific visual cycle. *Prog Retin Eye Res*, *30*(2), 115-128. https://doi.org/10.1016/j.preteyeres.2010.11.001
Webster, A. R., Héon, E., Lotery, A. J., Vandenburgh, K., Casavant, T. L., Oh, K. T., Beck, G., Fishman, G. A., Lam, B. L., Levin, A., Heckenlively, J. R., Jacobson, S. G., Weleber, R. G., Sheffield, V. C., & Stone, E. M. (2001). An analysis of allelic variation in the ABCA4 gene. *Invest Ophthalmol Vis Sci*, *42*(6), 1179-1189.
Weng, J., Mata, N. L., Azarian, S. M., Tzekov, R. T., Birch, D. G., & Travis, G. H. (1999). Insights into the function of Rim protein in photoreceptors and etiology of Stargardt's disease from the phenotype in abcr knockout mice. *Cell*, *98*(1), 13-23. https://doi.org/10.1016/s0092-8674(00)80602-9
Westeneng-van Haaften, S. C., Boon, C. J., Cremers, F. P., Hoefsloot, L. H., den Hollander, A. I., & Hoyng, C. B. (2012). Clinical and genetic characteristics of late-onset Stargardt's disease. *Ophthalmology*, *119*(6), 1199-1210. https://doi.org/10.1016/j.ophtha.2012.01.005
Xie, T., Zhang, Z., Fang, Q., Du, B., & Gong, X. (2021). Structural basis of substrate recognition and translocation by human ABCA4. *Nat Commun*, *12*(1), 3853. https://doi.org/10.1038/s41467-021-24194-6
Zernant, J., Lee, W., Collison, F. T., Fishman, G. A., Sergeev, Y. V., Schuerch, K., Sparrow, J. R., Tsang, S. H., & Allikmets, R. (2017). Frequent hypomorphic alleles account for a significant

fraction of ABCA4 disease and distinguish it from age-related macular degeneration. *J Med Genet*, *54*(6), 404-412. https://doi.org/10.1136/jmedgenet-2017-104540

Zhang, B. Z., Zhang, X., An, X. P., Ran, D. L., Zhou, Y. S., Lu, J., & Tong, Y. G. (2009). An easy-to-use site-directed mutagenesis method with a designed restriction site for convenient and reliable mutant screening. *J Zhejiang Univ Sci B*, *10*(6), 479-482. https://doi.org/10.1631/jzus.B0820367

Zhong, M., Molday, L. L., & Molday, R. S. (2009). Role of the C terminus of the photoreceptor ABCA4 transporter in protein folding, function, and retinal degenerative diseases. *J Biol Chem*, *284*(6), 3640-3649. https://doi.org/10.1074/jbc.M806580200

7. Supplementary data

7.1 Schematic representation of the pCEP4_ABCA4 (NM_000350) plasmid

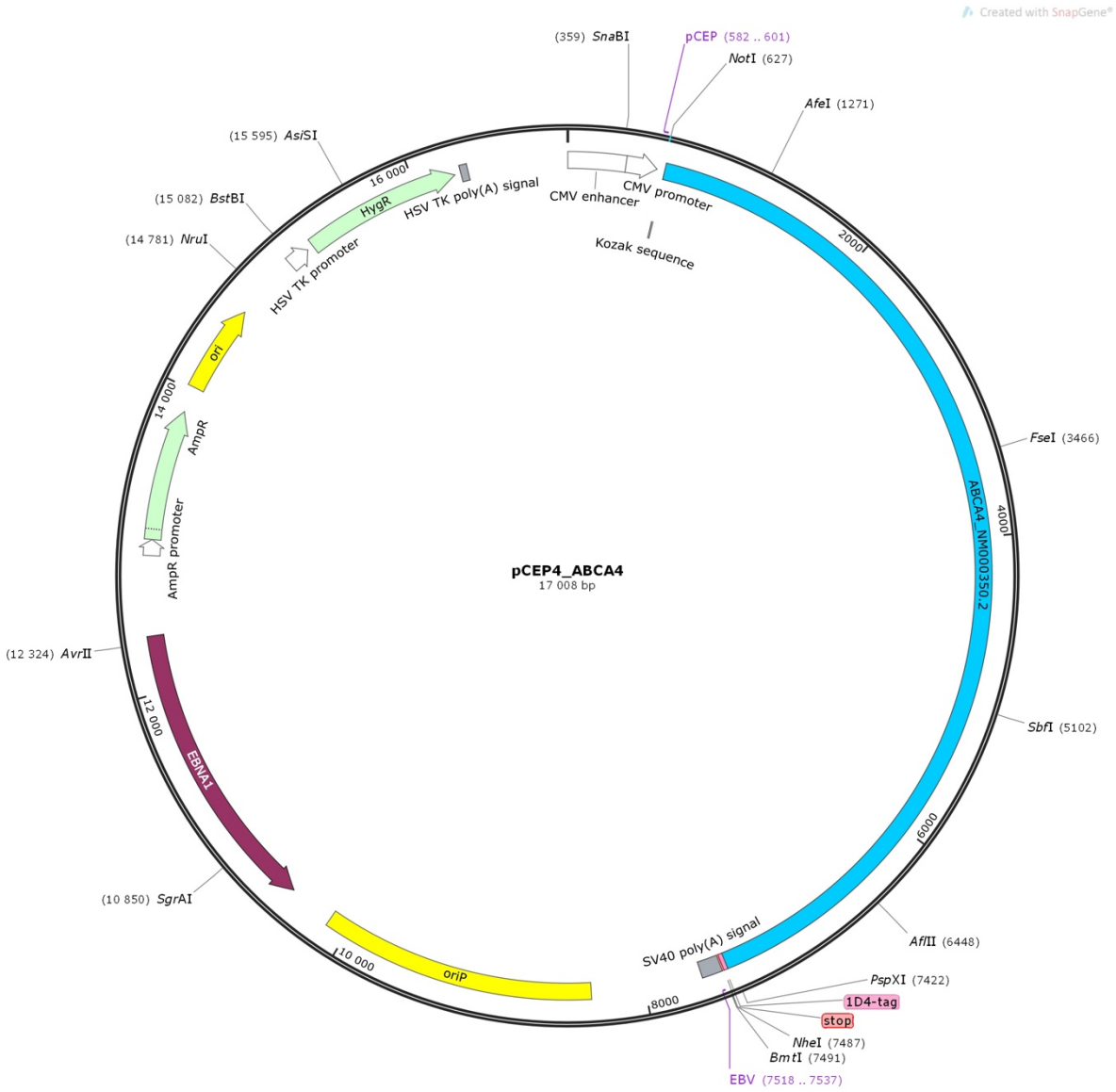

Figure 7.1: Schematic representation of the pCEP4_ABCA4 plasmid used for the expression of ABCA4. The blue represents the ABCA4 insert, and the position of the studied mutations is marked. The 1D4-tag has also been denoted, here highlighted in pink, and the restriction enzymes used in this study are denoted on either side of the insert.

7.2 Representative example of an agarose gel used for restriction mapping

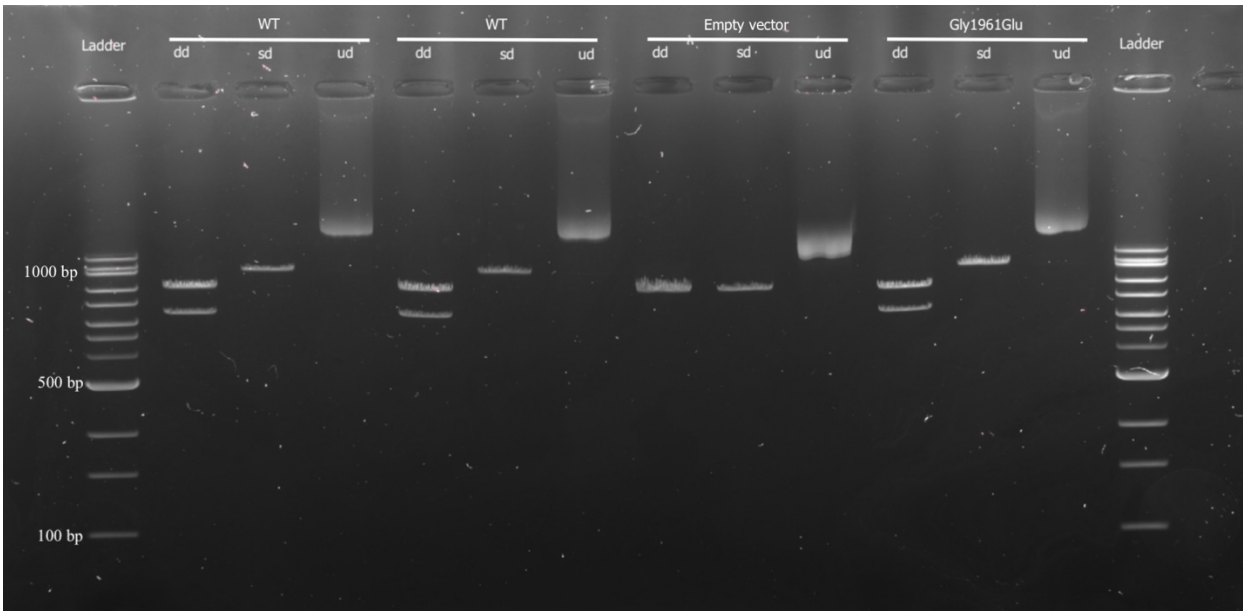

Figure 7.2 Representative example of an agarose gel used for restriction mapping of plasmids after maxiprep, prior to Sanger sequencing. Restriction mapping was performed to check the inserts after maxiprep. Each sample is denoted as marked over the wells. Two controls were run for each sample, single digested samples were only subjected to NheI and undigested samples were not subjected to any restriction enzymes. 100 ng plasmid DNA was loaded onto each well. Each sample showed two bands for the double digested samples, corresponding to the insert and the vector, meaning that the ABCA4 insert had been successfully inserted. dd: double digested, sd: single digested, ud: undigested